NASA Technical Memorandum 81399

CHEMICAL PROCESSES INVOLVED IN THE INITIATION OF HOT CORROSION OF B-1900 AND NASA-TRW VIA

George C. Fryburg, Fred J. Kohl,
and Carl A. Stearns
Lewis Research Center
Cleveland, Ohio

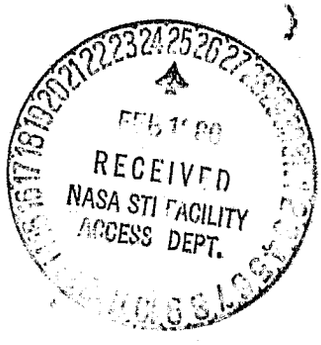

Prepared for the
One hundred fifty-sixth Meeting of the
Electrochemical Society
Los Angeles, California, October 14-19, 1979

CHEMICAL PROCESSES INVOLVED IN THE INITIATION OF HOT CORROSION OF B-1900 AND NASA-TRW VIA

by George C. Fryburg, Fred J. Kohl, and Carl A. Stearns

National Aeronautics and Space Administration
Lewis Research Center
Cleveland, Ohio 44135

E-308

SUMMARY

Sodium sulfate-induced hot corrosion of B-1900 and NASA-TRW VIA at 900° C has been studied with special emphasis on the chemical reactions occurring during and immediately after the induction period. Thermogravimetric tests were run for set periods of time after which the samples were washed with water. Information was obtained by chemical analysis of water soluble metal salts and of residual sulfate. Companion samples were run, cross-sectioned dry, and polished in Varsol. Element distributions within the oxide layer were obtained from electron microprobe X-ray micrographs. A third set of samples was subjected to surface analysis by ESCA. Evolution of $SO_2(g)$ was monitored throughout many of the hot corrosion tests. Results are interpreted in terms of acid-base fluxing mechanisms.

INTRODUCTION

The problem of hot corrosion attack on gas turbine components exposed to combustion gases has persisted for many years. The attack is encountered under circumstances where intake air and/or fuel is contaminated with airborne salt or sea salt. The hot corrosion is usually attributed to attack by sodium sulfate which is formed by reaction in the turbine combustor between ingested sodium chloride and sulfur contained in the fuel. It is anticipated that the problem will be aggravated by the use of higher operating temperatures and pressures in modern day gas turbines. Additional contributions to such attack can be expected by the increased use of wider specifications on aircraft turbine fuels and of cheaper, dirtier fuels in industrial/utility turbines.

Most nickel-base superalloys are susceptible to hot corrosion attack to some extent. The hot corrosion phenomenon is complex and depends on many factors: temperature, composition of alloy, cyclic conditions, impurities in and pressure of air ingested into engine, and impurities in the fuel burned by the engine. Because of the complexity of the problem, various laboratory tests have been devised to simulate hot corrosion so that certain aspects of the problem can be

isolated and studies in detail (Refs. 1, 2 and 3). In the work described below, hot corrosion was induced by coating metal samples with Na_2SO_4 and oxidizing them at elevated temperatures. The course of the hot corrosion was followed gravimetrically, as reported previously (Refs. 4 and 5).

Induced hot corrosion of superalloys displays two types of behavior: "catastrophic," in which the oxidation proceeds at an approximately linear rate until the sample is largely consumed; or "accelerated," in which the oxidation is enhanced over that normally encountered but finally the rate decreases at longer times (Refs. 5 and 6). The type of behavior exhibited depends on alloy composition, temperature, and amount of Na_2SO_4 applied (Refs. 4 and 5). Usually, attack is preceded by an induction period during which little or no weight gain is observed (Ref. 5). However, once hot corrosion begins, it proceeds to such an extent that the structural integrity of the alloy is compromised. It appears that prevention of hot corrosion must be attained by prevention of the initiation reactions that occur during the induction period. We have been investigating the processes that occur during the induction period using two nickel-base alloys: B-1900 and NASA-TRW VIA. Some of the preliminary results for B-1900 were reported previously (Ref. 5).

EXPERIMENTAL

The alloy samples of B-1900 and NASA-TRW VIA were obtained from commercial sources and were given conventional heat treatments. A modified B-1900 alloy, in which the molybdenum was replaced on a weight basis by tantalum, was made in-house. Accurately weighed powders were vacuum melted and cast in a copper mold. Chemical analyses of the alloys are presented in Table I. Test samples were coupons measuring 0.3x1.0x2.5 cm with a hangdown hole in one end. All surfaces were glass-bead blasted to give a uniform matte finish. The coupons were cleaned ultrasonically in trichloroethylene, detergent, distilled water, acetone, and ethanol, and then dried in an oven at 120° C.

All samples were preoxidized in a temperature-regulated tube furnace is slowly flowing oxygen at 900° C for 100 h. The preoxidation treatment increased the length of the induction period compared with unoxidized specimens, allowing greater time resolution in our measurements (Refs. 4 and 5). Hot corrosion was induced by coating the preoxidized samples with 3 ($\pm$5%) mg cm^{-2} of Na_2SO_4, followed by isothermal oxidation at 900° C. The Na_2SO_4 was applied by air brushing a saturated solution of Na_2SO_4 onto the coupons, heated on a hot plate to 200° C. The oxidation was performed in a vertical tube furnace. The direction of flow of oxygen was downward in the quartz furnace tube and the speed was 20 cm min^{-1}. Continuous gravimetric measurements were made with a Cahn R-100 microbalance. Corrections in the weight change were made for flow and buoyancy effects.

Samples were run for set periods of time and the hot corrosion process was stopped by air cooling to room temperature. After exposure, one set of samples of each alloy was washed for 15 minutes in hot water, and the resulting solutions were analyzed for $SO_4^=$ and metal cations and/or anions by atomic absorption methods. The $SO_4^=$ was determined by the X-ray fluorescence method of Luke (Ref. 7), modified to allow precipitation times of five hours or longer. The method involves precipitation of $SO_4^=$ as $BaSO_4$ and determination of the amount of $SO_4^=$ by monitoring the K_α X-ray fluorescence of sulfur. Some interference from molybdenum may occur for the long time samples in which sulfate was low and soluble molybdenum was high. Interference results from the inability to resolve the K_α sulfur and the L_α molybdenum X-ray lines. The effect was generally found to be small. Where molybdenum interference was indicated by detection of its L_β fluorescence, which was resolvable, a correction was made in the intensity of the sulfur K_α line using the previously determined L_α/L_β intensity ratio for the molybdenum lines.

For B-1900, a second set of samples was mounted and cross-sectioned for morphological examination of the oxide scale by light microscopy and the electron microprobe. These samples were coated with copper in an electron beam evaporator, cross-sectioned dry over an eight-hour period, and polished by using trichloroethylene or Varsol as a medium. Individual compounds were identified from elemental X-ray micrographs on the basis of X-ray diffraction analyses previously reported (Refs. 4 and 5).

Surface analyses of hot corroded samples were obtained by X-ray photoelectron spectroscopic techniques (ESCA) in a cooperative effort with Case Western Reserve University under NASA Grant NSG-3009. Samples were examined with a Varian IEE-15 X-ray photoelectron spectrometer equipped with a high intensity magnesium anode (K_α-radiation, 1253.6 eV). Binding energies were corrected for surface-charging effects by reference to the C 1S (hydrocarbon contamination) peak, which was assigned the standard binding energy of 285.0 eV. The estimated uncertainty of the measured binding energy was $\pm$0.2 eV for simple peaks. Because of the cylindrical symmetry of the spectrometer, the ESCA corrosion samples were cylindrically shaped, consisting of two sections designed for insertion into the chuck sample holder of the spectrometer. The main body section was 1.9 cm high and 1.1 cm in diameter; the upper section was 0.4 cm high and 0.25 cm in diameter. A 0.15 cm diameter hole through the upper section allowed hanging the sample in the hot corrosion apparatus. Samples were stored in desiccators after the corrosion treatment prior to ESCA analysis. Details of the apparatus and procedure are described in Reference 8.

In many of the experiments performed with B-1900, the concentration of SO_2 was determined in the oxygen flowing out of the furnace tube during the hot corrosion run. The SO_2 was measured with a Thermoelectron Pulsed Fluorescent SO_2 Analyzer which is specific to SO_2 and is insensitive to flow and temperature of the carrier gas. The analyzer measures

SO_2 on a continuous basis. The principle of operation is based on the excitation of fluorescence of SO_2 molecules by pulsed ultraviolet radiation. The detection capability extended from 0.01 to 50 ppm by employing four different instrument ranges. The effluent from the furnace tube was conducted into the SO_2 analyzer through stainless steel fittings and teflon tubing. For these experiments, the oxygen flow through the furnace tube had to be increased to 620 ml min^{-1} from 100 ml min^{-1}. This change in oxygen flow rate had no detectible effect either on the microbalance performance or on the course of hot corrosion.

RESULTS AND DISCUSSION

Thermogravimetric. - Both B-1900 and NASA-TRW VIA are alloys that are classified as "alumina formers"; that is, their oxidation resistance results from the formation of a thin dense protective oxide composed largely of α-Al_2O_3 (Ref. 9). Generally, alumina formers are more susceptible to hot corrosion than "chromia formers," i.e., alloys that derive their oxidation resistance from a protective oxide layer composed largely of Cr_2O_3. The comparative hot corrosion behavior of four nickel-base superalloys (B-1900, 713C, NASA-TRW VIA, and IN738) is shown in Figure 1 where we have plotted the specific weight gain against exposure time (Ref. 4). The samples were preoxidized for 100 hours at 900° C and corroded at the same temperature after application of 3 mg cm^{-2} Na_2SO_4. The two alumina formers and 713C[1] corroded catastrophically while the chromia former, IN738, was hardly affected.

Hot corrosion of alumina formers is usually manifested as a localized attack that starts at one spot and spreads laterally across the sample. This is depicted in Figure 2 by the sample corroded for seven hours. Attack has commenced on the left edge and is moving across the face of the sample. The sample corroded for four hours shows no noticeable attack, and a blob of Na_2SO_4 is evident along the bottom edge. The localized nature of the attack must be taken into account in interpreting the oxide morphologies.

A typical hot corrosion curve for B-1900 is shown in Figure 3a where the specific weight gain is plotted against the time. The weight gain is plotted with two sensitivities to elucidate the details of kinetics. The beginning of the hot corrosion process is characterized by a period of no weight gain; in fact, with preoxidized samples, a slight weight loss is observed. Actually, the duration of the induction period is a function of the test temperature, composition of the alloy, amount of Na_2SO_4, and preoxidation treatment of the sample. In our

---

[1] Alloy 713C is an alumina former when oxidized in air (Ref. 10), but our previous results (Ref. 9) showed that it behaved as a chromia former when oxidized in oxygen at 900° C.

preliminary report (Ref. 5), we arbitrarily defined the length of the induction period as the time when the sample had gained 0.3 mg cm^{-2}. In this report, we redefine it as the time when the abrupt change in slope occurs in the corrosion curve. As shown by the X10 curve in Figure 3a, this time is six and one-quarter hours, and the specific weight gain is about 0.8 mg cm^{-2}.

The induction period is followed by a short region in which the rate approximates parabolic behavior, and results in a "foot" in the X1 corrosion curve. The rate accelerates gradually, reaching a region in which linear behavior is displayed. This linear attack region continues as the sample is consumed and a thick scale develops. Finally, the rate falls off as a consequence of these two effects.

The corrosion curve for VIA, shown in Figure 4a, is somewhat different from that for B-1900. The induction period is much longer, being about 15 hours, and the "abrupt change" in the slope is less pronounced. For VIA, the whole corrosion process is more protracted.

Water Soluble Elements. - Samples of B-1900 and VIA were corroded for set periods of time after which water soluble elements were extracted. Because the length of the induction period varied somewhat among individual samples, the actual times were normalized by matching the weight gain with the curves given in Figures 3a and 4a for the two alloys. For B-1900, samples were run for every hour up to 12 hours and less frequently thereafter; for VIA, every four hours except around the end of the induction period where they were run more frequently. The results are shown in Figures 3b and 4b for B-1900 and VIA, respectively. We have plotted the amount found, in milligrams, of each element and $SO_4^=$ against the time of corrosion. Individual points have been eliminated for clarity and the data are presented as smoothed curves. The weights of $SO_4^=$ and Na^+ originally applied to the samples are given at zero time: about 24 mg of Na_2SO_4 for B-1900 and 21 mg for VIA, depending on sample area. All amounts of soluble elements were normalized to these amounts of Na_2SO_4.

The analytical results for the two alloys are in general agreement. Sodium was essentially recovered completely except at long times when it became imbedded in thick scales or tied up in only slightly soluble compounds such as $NaTaO_3$ and Na_2TiO_3. Most of the $SO_4^=$ was recovered for times up to near the end of the induction period after which the amount decreased rapidly to less than 10 percent of its original value. Soluble aluminum appears at the end of the induction period, maximizes rapidly, and disappears. The presence of soluble aluminum probably indicates that the protective layer of Al_2O_3 on the alloys is being dissolved. The disappearance of soluble aluminum results from reformation of Al_2O_3, but not as a protective layer. Soluble chromium appears very early in the hot corrosion process and is evidenced by the yellow chromate color associated with the Na_2SO_4 found remaining on the surface of the cooled samples. Chromium exhibits a broad shallow maximum and finally disappears, indicating reformation of Cr_2O_3.

The most striking feature of the results, especially for B-1900, is the behavior of soluble molybdenum. A small amount of molybdenum appears shortly before the end of the induction period, but the amount increases rapidly to a very large value just after the induction period. On first thought, one might not expect soluble molybdenum to exceed that required to tie up the available sodium as Na_2MoO_4. However, the oxide MoO_3 itself is also water soluble to the extent of 2 g in 100 ml of water at 70° C. Thus, considerable molybdenum has been oxidized at this stage in the hot corrosion process. The smaller quantity of molybdenum found for VIA is in keeping with its lower molybdenum content: 2 wt % in VIA compared with 6 wt % in B-1900. In addition, some soluble tungsten is evident.

Sometime after the induction period, soluble nickel appeared in the B-1900 extracts, increasing monotonically with time. Just detectible quantities of cobalt were also evident at this time. No soluble titanium was detected, but small amounts of tantalum were detected prior to the end of the induction period for the VIA samples.

Sulfur Dioxide Evolution. - The SO_2 evolving during the hot corrosion process was measured for several B-1900 samples. The results are shown in Figure 5b where the concentration of SO_2 in ppm detected in the oxygen is plotted against the corrosion time. Some SO_2 was evolved from the sample as soon as it was brought up to the test temperature. The concentration rose rapidly to about 3 ppm, and gradually decreased, reaching zero after about four and one-half hours. It remained at zero until about one-half hour after the end of induction period at which time a small burst occurred to about the 0.5 ppm level and that lasted for about 10 minutes. No more SO_2 was evolved after that until the corrosion rate started accelerating, reaching the region of linear rate. At this time, a large concentration of SO_2 was observed, attaining a value of approximately 15 ppm. This value was maintained for one to two hours and then decreased to a very low value, <0.04 ppm.

It is instructive to relate the instantaneous concentrations of SO_2 observed to the total amount of SO_2 evolved during the corrosion process; that is, to integrate the concentrations over the time. These results are presented in Figure 5c where the amount of SO_2 evolved after a given corrosion time is expressed in terms of the equivalent milligrams of $SO_4^=$ required. The equivalent sulfate was calculated on the basis that the sulfur evolved as 3/4 SO_2 and 1/4 SO_3[2]. For comparison, we also present in Figure 5c the amount of water soluble $SO_4^=$ recovered (from Fig. 3b). It can be seen from Figure 5c that about 11 mg of the originally applied 17 mg was evolved as SO_2-SO_3 gases during the course of the hot corrosion. Roughly, 2 mg came off during the first 2/3 of the

---

[2]Thermodynamic equilibrium calculations indicated that at 900° C the ratio SO_3/SO_2 in one atmosphere of oxygen is about 0.32, so that roughly three-quarters of the sulfur oxide gases formed would evolve as SO_2.

induction period and the other 9 mg during the early part of the region in which the rate was linear. The remaining $SO_4^=$ probably was converted to sulfides of chromium which still remained in the unoxidized alloy. Eventually even these sulfides oxidized and the sulfur evolved as SO_2-SO_3. This was observed as a constant low level of SO_2 evolution until the sample was almost completely consummed.

Microprobe Analysis. - Samples were mounted and cross-sectioned for microprobe examination by using dry techniques so that water soluble compounds, especially sodium compounds, were not removed. Most of this work was done with B-1900 samples. As a test of the efficacy of the techniques, a sample was prepared that had been corroded for only 15 minutes. This sample also served as a point of reference for the other B-1900 samples corroded for longer times. The secondary electron and elemental X-ray micrographs are displayed in Figure 6. The micrographs show that the sample is covered with a thin continuous protective oxide composed largely of Al_2O_3 which, in turn, is covered with a layer of Na_2SO_4.

The micrographs of samples corroded for one and two hour periods were similar to that of the 15 min sample. Even the micrograph of the three hour sample showed only one small area where some attack had taken place: the micrographs of this area are depicted in Figure 7. The area is near the bottom of the sample and the Na_2SO_4 drop is evident on the surface. Examination of the Na_2SO_4 shows the presence of dissolved chromium and some molybdenum. The protective Al_2O_3 layer has changed: TiO_2 is lying along the outer surface; internal oxidation of aluminum has occurred, indicated by the aluminum-rich "tentacles;" and Cr_2O_3 has formed. Interaction with the Na_2SO_4 is indicated by the numerous, small internal sulfides lying under the oxide in the alloy.

In the four-hour sample, areas of the type depicted in Figure 7 became more numerous. In addition, one area, shown in Figure 8, was observed in which the Na_2SO_4 appears to be just penetrating the protective oxide. This has resulted in oxidation of molybdenum, titanium, chromium, and aluminum in the alloy just below the original Al_2O_3 layer. Internal sulfides, resulting from interaction with Na_2SO_4, are especially abundant.

In the five-hour sample, the areas of Na_2SO_4 penetration become more abundant and extend further into the alloy as shown in Figure 9 The sulfides are even more prominent and match up with areas on the aluminum and chromium X-ray micrographs.

By the end of the induction period, 6.25 hours, the Na_2SO_4 penetration encompasses nearly one-half of the surface area. As shown in Figure 10, the depth of penetration has increased and the alloy in this region has been completely stripped of alloying elements leaving areas of pure nickel/cobalt. Internal sulfides are still numerous and increasing in the alloy below the scale. In addition, an elliptical

nickel sulfide particle is evident in the upper portion of the scale at the far right. However, none of these features can explain the sudden large decrease in recoverable sulfate that occurs at this time.

Prior to mounting, examination of this 6.25-hour sample revealed a circular area of attack roughly 1 cm in diameter situated in the upper half of the sample. The sample was subsequently cross-sectioned so that the edge of this area was exposed. A light micrograph of this corrosion front is presented in Figure 11. The large shiny areas comprising nearly one-third of the scale are shown to be nickel sulfide by the elemental X-ray micrographs of the central portion of the scale presented in Figure 12. These large sulfides are, of course, molten at the corrosion temperature and are penetrating the oxide as they migrate across the sample. The occurrence of such massive nickel sulfides can account for the disappearance of the $SO_4^=$. The liquid Na_2SO_4 has broken through the protective oxide at this point and the metallic nickel has reacted with it to form sulfides. As the molten Na_2SO_4 is removed at the reaction site, additional sulfate is drawn by surface tension from others parts of the sample, especially from the drop hanging around the bottom.

After seven hours of corrosion, the massive nickel sulfides are still prominent (with pure nickel areas in the center)(Fig. 13). The new feature that is evident at this time is the appearance of a MoO_3 layer underneath the scale adjacent to the alloy. Higher magnification of this area (Fig. 14) shows that sodium is present in the MoO_3, especially in the upper portion. This probably means that Na_2MoO_4, because of its high thermodynamic stability, is dissolved in the MoO_3. Both of these compounds would be molten at the corrosion temperature so that the layer would spread underneath the oxide scale. The X-ray micrographs show that chromium, aluminum, and even nickel are dissolved in the molten Na_2MoO_4-MoO_3 layer.

After 10 hours of corrosion exposure, the scale has increased markedly in thickness (Fig. 15). Residual nickel sulfides are still present but are much reduced in size while chromium sulfides are situated down in the alloy. The Na_2MoO_4-MoO_3 layer is prominent underneath the scale. Even at this stage in the corrosion, areas are present where attack is characteristic of much earlier times (Fig. 16), emphasizing the localized nature of the processes.

After 20 hours, the main feature is the migration of the Na_2MoO_4-MoO_3 molten layer progressing across the sample underneath the oxide scale (Fig. 17). The direction of attack is from left to right.

While less extensive work has been done with the VIA alloy, it appears that the hot corrosion attack results in morphological features similar to those found with B-1900. Figure 18 shows the X-ray micrographs for a VIA sample corroded for 17.5 hours, a time just after the end of the induction period. The Na_2MoO_4-MoO_3 layer is prominent and

is progressing under the oxide scale from right to left. This sample was cut and polished by using standard wet techniques so that no sodium X-ray micrographs were obtainable. Nevertheless, the morphology is very similar to that of B-1900 samples at the same stage of corrosion.

ESCA Analysis. - X-ray photoelectron spectroscopy, widely known as ESCA, affords a useful technique for the study of solid surfaces. It is responsive to all elements except hydrogen and is sensitive to differences in chemical environment enabling the identification of different oxidation states. It samples just the first few atomic layers of a surface.

The surface analysis of a set of B-1900 samples hot corroded at 900° C with 3 mg cm^{-2} Na_2SO_4 is presented in Figure 19. The elemental abundance is given relative to that of sodium and is plotted against the time of corrosion. The results show that significant amounts of aluminum, chromium, nickel, and titanium are transferred from the oxide layer to the surface of the salt layer early in the induction period, that is, after one-half hour. It is not possible to determine if these elements are dissolved in the Na_2SO_4 or exist as an oxide slag (Ref. 6) floating on the Na_2SO_4. More details of this work are presented in Reference 8.

The atomic abundance of sulfur (identified as $SO_4^=$ by its binding energy) is close to the stoichiometric value for Na_2SO_4 up to near six hours, after which it falls rapidly. This behavior is similar to that of the water soluble sulfate.

One of the objectives of the ESCA work (Ref. 8) was to try to identify aluminum in the AlO_2^- - or in $Al_2(SO_4)_3$ - like environments on the surface of corroding samples. Standard spectra obtained with $NaAlO_2$, $Al_2(SO_4)_3$, and $NaAl(SO_4)_2$ showed that the Al 2S binding energy (E_b) for $NaAlO_2$ was only 0.3 eV lower than that of Al_2O_3; but that for $Al_2(SO_4)_3$ and $NaAl(SO_4)_2$, the E_b was 1.3 and 1.4 eV higher, respectively, relative to Al_2O_3. Thus, AlO_2^- could not be established or ruled out because the shift in E_b was close to the uncertainty of the measurements ($\pm$0.2 eV). However, detection of Al^{+3} in environments similar to that in $Al_2(SO_4)_3$ and $NaAl(SO_4)_2$ should be feasible. The search for this shifted Al^{+3} on the surface of corroded samples was not successful - only Al^{+3} in Al_2O_3 was observed. Because any soluble Al^{+3} formed at the salt/alloy interface would likely reform as Al_2O_3 at the salt/oxygen interface, this result may not be surprising. This suggests that the search should be continued toward the salt/alloy interface by mechanical removal of peripheral layers.

It was possible to distinguish between Cr^{+3} and Cr^{+6} on the basis of their different binding energies. The spectra revealed that Cr^{+6} was the predominant species in the surface after the first half hour, and that its proportion increased up to the end of the induction period,

reaching about 80 percent of the total chromium observed (Ref. 8). This is in general agreement with the water soluble chromium determinations.

Chemical Mechanisms. - The results of these studies of Na_2SO_4-induced hot corrosion of two nickel-base alloys that form principally alumina scales can be interpreted in terms of the following sequence of reactions. Interpretation is couched within the framework of the acid-base fluxing mechanism of Na_2SO_4 (Refs. 1, 3, 6, and 11). A summary of our mechanism is given in Table IX and Figure 20.

Initially, some of the Cr_2O_3 on the preoxidized samples is oxidized to soluble chromate:

$$Cr_2O_3 + 3/2\ O_2(g) + 2Na_2SO_4(\ell) \rightarrow 2Na_2CrO_4(\ell) + 2SO_3(g) \qquad (1)$$

This reaction continues throughout the induction period consuming around 4 mg of $SO_4^=$ (based on 2 mg of soluble Cr, Fig. 3b) and releasing the sulfur as gaseous SO_2 and SO_3.

Subsequently, MoO_3 that has formed under the Na_2SO_4 liquid layer by oxidation of surface carbides (Ref. 6) reacts with the sulfate:

$$MoO_3(\ell) + Na_2SO_4(\ell) \rightarrow Na_2MoO_4(\ell) + SO_3(g) \qquad (2)$$

It is difficult to determine to what extent this reaction proceeds based on the soluble molybdenum found because both MoO_3 and Na_2MoO_4 are water soluble. Because the large drop in sulfate (Figs. 3 and 4) occurs before the rapid rise in soluble molybdenum, reaction (2) probably does not proceed to a large extent during the induction period. The major portion of the Na_2MoO_4 observed in the micrographs of the after-induction period samples probably results from reaction of MoO_3 with other sodium-containing salts with lower thermodynamic stabilities than Na_2MoO_4. It should be noted that both reactions (1) and (2) tend to increase the "acidity" of the Na_2SO_4.

At the end of the induction period the $SO_4^=$ is decreasing rapidly and nearly half of it has been consumed (Figs. 3 and 4). This is an indication that the protective Al_2O_3 scale has been breached at some localized spot such as that shown on the four-hour sample (Fig. 8), and that the underlying nickel is reacting with the Na_2SO_4:

$$Ni + SO_4^= \rightarrow NiS(\ell) + 3/2\ O_2(g) + O^= \qquad (3)$$

The Na_2SO_4 is drawn into the reaction site, probably by surface tension, producing the large NiS areas observed on the 6.25-hour and later samples (Figs. 11 to 14).

It seems plausible that the other elements of the alloy can also react with the Na_2SO_4, for example

$$2Al + 3SO_4^{=} \rightarrow Al_2O_3 + 3SO_2(g) + 3O^{=} \quad (4)$$

$$2Cr + 3SO_4^{=} \rightarrow Cr_2O_3 + 3SO_2(g) + 3O^{=} \quad (5)$$

Similar reactions can occur with the minor constituents of the alloy: titanium, tantalum, and molybdenum. It should be noted that oxides of all these elements will most probably be formed rather than sulfides, as is the case for nickel. This results from the greater stability of these oxides compared to their sulfides under low partial pressures of oxygen, as shown by Gulbransen and Meier (Ref. 12). Cobalt, which might be expected to behave like nickel, appears to form the oxide under these conditions. No sign of cobalt was found in the sulfide areas, only nickel (see Fig. 12). Evidence for the occurrence of these reactions is shown in the micrographs by the presence of all these alloy elements in the Na_2SO_4 found below the original oxide scale (Figs. 9 and 10). Nevertheless, the oxide ions are produced mainly by reaction (3) because of the preponderance of nickel in the alloy.

The production of large concentrations of oxide ion allows basic fluxing of the Al_2O_3 on adjacent areas of the sample:

$$Al_2O_3 + O^{=} \rightarrow 2AlO_2^{-} \quad (6)$$

and the attack spreads laterally. Reaction (6) accounts for the appearance of soluble aluminum right after the induction period (Figs. 3 and 4). However, as the oxide ion is used up, the attack slows down as indicated by the foot in the X1 hot corrosion curve and by the maximum in the soluble aluminum (Fig. 3). At longer times, from eight to ten hours, the Al_2O_3 and Cr_2O_3 are reprecipitated as evidenced by the decrease in the soluble aluminum and chromium (Fig. 3). This may, in part, be due to consumption of the oxide ions by the MoO_3 which is increasing rapidly at this time, as indicated by the molybdenum curve of Figure 3:

$$MoO_3(\ell) + O^{=} \rightarrow MoO_4^{=} \quad (7)$$

$$2NaAlO_2 + MoO_3(\ell) \rightarrow Al_2O_3 + Na_2MoO_4(\ell) \quad (8)$$

$$2Na_2CrO_4(\ell) + 2MoO_3(\ell) \rightarrow Cr_2O_3 + 2Na_2MoO_4(\ell) + 3/2\ O_2(g) \quad (9)$$

As these reactions proceed, the MoO_3 phase is enriched with Na_2MoO_4 as shown in the X-ray micrographs depicted in Figures 13, 14, and 15. The Na_2MoO_4 acts to reduce the loss of molybdenum by vaporization of

MoO_3[3] and stabilizes the molten Na_2MoO_4-MoO_3 phase. At this point in time most of the sulfate has reacted as shown in Figure 3 so that the corrosive molten phase is largely Na_2MoO_4-MoO_3. This Na_2MoO_4-MoO_3 phase can effect acidic fluxing of the protective oxides Al_2O_3 and Cr_2O_3:

$$Al_2O_3 + 3MoO_3(\ell) \rightarrow 2Al^{+3} + 3MoO_4^{=} \quad (10)$$

$$Cr_2O_3 + 3MoO_3(\ell) \rightarrow 2\ Cr^{+3} + 3MoO_4^{=} \quad (11)$$

This acidic fluxing is self sustaining and accounts for the acceleration of the corrosion rate from parabolic (from 6.25 to 9 hours, Fig. 3) to linear as the molten Na_2MoO_4-MoO_3 migrates across the sample compromising any protective scale. This disruption of the scale by the Na_2MoO_4-MoO_3 also allows oxidation of the NiS that was formed at the end of the induction period:

$$NiS(\ell) + 3/2\ O_2(g) \rightarrow NiO + SO_2(g) \quad (12)$$

The NiS oxidation continues for several hours, releasing relatively large amounts of $SO_2(g)$, as shown in Figure 5b. The internal sulfides that are evident in the micrographs of the corroded samples probably do not oxidize to yield SO_2 at this time. Spengler and Viswanathan (Ref. 13) have shown that oxidation of these internal chromium sulfides liberates sulfur which nucleates new sulfide particles along a front advancing into the alloy substrate. However, if the alloy were totally consumed these sulfides would eventually oxidize, liberating SO_2 also. Eventually, the corrosion rate drops off from linear at long times as the sample is consumed.[4]

---

[3]We estimate that the vapor pressure of Na_2MoO_4 is about 10^8 less than that of MoO_3 at 1200 K.

[4]If hot corrosion is induced with smaller amounts of Na_2SO_4 (1 mg cm^{-2} or less), accelerated oxidation results instead of catastrophic oxidation (Refs. 4 and 5). The deceleration of the linear rate is effected by conversion of liquid MoO_3 to solid $NiMoO_4$:

$$MoO_3(\ell) + NiO \rightarrow NiMoO_4 \quad (13)$$

The occurrence of reaction (13) was evidenced by the prominent $NiMoO_4$ X-ray diffraction patterns (JCPOS Card No. 16-291) exhibited by all samples hot corroded for long times; in fact, the oxides peeled off just above this $NiMoO_4$ layer (Ref. 4). Similar behavior was observed by Bourhis and St. John (Ref. 14) for IN713LC and IN100, two other alumina formers containing molybdenum. The catastrophic oxidation encountered with larger amounts of Na_2SO_4 probably results because Na_2MoO_4 forms a larger fraction of the molten phase, and removal of $MoO_3(\ell)$ by reaction (13) was not as critical as with smaller amounts of Na_2SO_4.

This chemical mechanism differs from the one previously proposed (Ref. 5) which was based on our preliminary results with B-1900. In the former mechanism, we postulated that the sulfate was removed by reaction (2), lowering the oxide ion concentration until acid fluxing of the Al_2O_3 occurred by reaction (10). The discovery of the large quantities of NiS formed in the reaction front of the 6.25 hour B-1900 sample (Figs. 11 and 12) indicates that the oxide ion concentration must be increasing at this time (reaction (3)). In addition, the soluble molybdenum has only increased to around 2 mg at this time (Fig. 3) and could account for removal of only 2 mg of $SO_4^{=}$ (by reaction (2)). Based on this new evidence, it appears more reasonable to assume that the Al_2O_3 is initially dissolved by basic fluxing (reaction (6)) and that acid fluxing (reaction (10)) becomes important after the maximum in soluble aluminum has been reached, that is, after about nine hours (Fig. 3).

The morphological features of alloys that have undergone acidic or basic fluxing are different and fairly distinctive. Light micrographs of scales typical of basic fluxing and acidic fluxing are presented in Figure 21. The scale formed by basic fluxing is thinner than that formed by acidic fluxing. It consists of two distinct parts: the original outer scale formed during the preoxidation, though thicker than before; and an internal oxidation area where Na_2SO_4 has penetrated the outer oxide. This latter area contains oxides of all the elements in the alloy except nickel and cobalt. These elements are left behind in the remaining areas. Figure 10 shows X-ray micrographs of an area similar to that shown in Figure 21a. Sulfides of either aluminum or chromium usually are present in the alloy below the attack area.

The scale formed by acidic fluxing is thick and exhibits a layered structure (Fig. 21b). Beneath the scale adjacent to the alloy lies the Na_2MoO_4-MoO_3 layer (Fig. 15 shows the X-ray micrographs of this area). The scale itself is composed of oxides of all the elements in the alloy and some nickel sulfides. Below the molybdenum-rich layer, some sulfides, probably chromium, are present in the alloy. The layered structure results from the cyclic operation of reactions (10) and (11) and their reverse reactions. After solution of the oxides in the molten Na_2MoO_4-MoO_3 by reactions (10) or (11), the metal cations diffuse to the outer zone of the melt where they are reoxidized by the higher oxygen potential. The cycle repeats as the alloy is consumed. The cyclic behavior of hot corrosion can be explained analogously by the Rapp-Goto model (Ref. 15) in which the attack occurs because of a negative solubility gradient of the corrosion product in the molten phase.

Tantalum-Modified B-1900. - To add credence to the conclusion that the catastrophic hot corrosion of B-1900 and VIA results from the molybdenum in the alloys, an alloy was made similar to B-1900 in which all the molybdenum was removed and replaced with an equivalent weight percentage of tantalum. Tantalum was chosen as the replacement element because it has been shown to tie up the sodium from the Na_2SO_4 in the form of stable, solid $NaTaO_3$ (Ref. 16):

$$Ta_2O_5 + Na_2SO_4(\ell) \rightarrow 2NaTaO_3 + SO_3(g) \qquad (14)$$

Comparative hot corrosion curves for B-1900 and the Ta-Modified B-1900 are presented in Figure 22. The data are for preoxidized samples coated with 3 mg cm^{-2} Na_2SO_4 and oxidized at 900° C. The catastrophic behavior exhibited by B-1900 has been eliminated in the modified B-1900, and the amount of corrosion after 100 hours has been greatly reduced.

Examination of cross-sectioned samples of the Ta-Modified B-1900 reveals that hot corrosion has progressed by a basic fluxing mechanism. This is illustrated in Figure 23 by the back-scattered electron micrograph of a sample that had been corroded for 100 hours, and in Figure 24 by a light micrograph of another area of this sample. An interesting feature displayed by the X-ray micrographs in Figure 23 is the large fraction of sodium that is tied up by the tantalum as $NaTaO_3$[5] in the outer portions of the scale.

These thermogravimetric and micrographic results confirm that molybdenum in B-1900 is deleterious with respect to hot corrosion, effecting the catastrophic behavior observed with this alloy. The same conclusion can probably be made for the VIA alloy. These results are in agreement with previous work. Goebel, Pettit, and Goward (Ref. 6) showed that alloys containing molybdenum underwent catastrophic hot corrosion and Peters, Whittle, and Stringer (Ref. 17) found that alloys containing three percent or more molybdenum displayed catastrophic attack.

CONCLUSIONS

A chemical mechanism is proposed for elucidating the course of laboratory-induced hot corrosion of nickel-base alloys that are aluminum formers. The mechanism explains all the diverse experimental results observed in this study.

The mechanism indicates that hot corrosion of these alloys is initiated by basic fluxing of the protective Al_2O_3 scale. The attack is localized but spreads over the sample until the Na_2SO_4 has all reacted. The sequential, catastrophic corrosion of these alloys results from the molybdenum content. The molybdenum forms a low melting phase (Na_2MoO_4-MoO_3) that removes the protective scales by acidic fluxing. The molybdenum phase migrates across the sample resulting in a linear reaction rate and finally in complete consumption of the sample. The self-sustaining feature is a consequence of the cyclic nature of the acidic fluxing.

---

[5]X-ray diffraction patterns of the surface of this sample displayed a strong pattern characteristic of $NaTaO_3$ (JCPDS Card No. 2-873).

While the mechanism pertains specifically to the interpretation of laboratory results, it is believed that the mechanism is applicable to the practical problem of hot corrosion encountered in gas turbine engines. The amount of Na_2SO_4 applied to our laboratory test specimens was roughly three times that generally observed in practice. But, one must remember that the values observed in practice are average values and that locally, larger deposits can exist. In addition, hot corrosion is a localized attack that subsequently progresses across the alloy.

ACKNOWLEDGEMENTS

The authors would like to thank Frank M. Terepka for obtaining the electron microprobe data, and Warren F. Davis and John T. Halloran for performing the chemical analyses.

REFERENCES

1. N. S. Bornstein and M. A. DeCrescente, Trans. AIME 245, 1947 (1969); N. S. Bornstein, M. A. DeCrescente, and H. A. Roth, Metall. Trans. 4, 1799 (1973).

2. J. Stringer, Ann. Rev. Mater. Sci. 7, 477 (1977).

3. N. S. Bornstein and M. A. DeCrescente, Metall. Trans. 2, 2875 (1971).

4. C. A. Stearns, F. J. Kohl, and G. C. Fryburg, NASA TN D-8461 (1977).

5. G. C. Fryburg, F. J. Kohl, and C. A. Stearns, in "Properties of High Temperature Alloys," Z. A. Foroulis and F. S. Pettit, Editors, p. 585, The Electrochemical Society, Princeton, NJ (1976); also NASA TM X-73479 (1976).

6. J. A. Goebel, F. S. Pettit, and G. W. Goward, Metall. Trans. 4, 261 (1973).

7. C. L. Luke, Anal. Chim. Acta 43, 245 (1968).

8. S. R. Smith, W. J. Carter, III, G. D. Mateescu, F. J. Kohl, G. C. Fryburg, and C. A. Stearns, Oxid. Metals, in press; also G. D. Mateescu and S. R. Smith, NASA CR-159553 (1979).

9. G. C. Fryburg, F. J. Kohl, and C. A. Stearns, NASA TN D-8388 (1977).

10. C. A. Barrett, G. J. Santoro, and C. E. Lowell, NASA TN D-7484 (1973).

11. C. S. Giggins and F. S. Pettit, Pratt and Whitney, Middletown, Conn., PWA-FR-11545, 1979. (AD-A072645)

12. E. A. Gulbransen and G. H. Meier, in "Tenth Materials Research Symposium on Characterization of High Temperature Vapors and Gases," J. W. Hastie, Editor, NBS-SP-561, Vol. 2, p. 1639 (1979).

13. C. J. Spengler and R. Viswanathan, Metall. Trans. 3, 161 (1972).

14. Y. Bourhis and C. St. John, Oxid. Met. 9, 507 (1975).

15. R. A. Rapp and K. S. Goto, Paper presented at the Second International Symposium on Molten Salts, The Electrochemical Society 1978 Fall Meeting, Pittsburgh, Pennsylvania, Oct. 18-19, 1978.

16. G. C. Fryburg, C. A. Stearns, and F. J. Kohl, J. Electrochem. Soc. 124, 1147 (1977).

17. K. R. Peters, D. P. Whittle, and J. Stringer, Corros. Sci. 16, 791 (1976).

TABLE I. - Composition of Superalloys

Element	Alloy					
	B-1900		NASA-TRW VIA		Ta-Modified B-1900	
	Composition					
	wt %	at. %	wt %	at. %	wt %	at. %
Nickel	64.5	62.5	62	64.5	66.7	64.5
Chromium	8.0	8.7	6.1	7.1	7.6	8.3
Aluminum	6.0	12.6	5.4	12.2	6.4	13.5
Titanium	1.0	1.2	1.0	1.3	0.8	1.0
Cobalt	10.0	9.6	7.5	7.7	10.0	9.6
Molybdenum	6.0	3.5	2.0	1.3	-----	-----
Tungsten	[a].1	-----	5.5	1.8	-----	-----
Tantalum	4.3	1.4	9.0	3.0	8.4	2.6
Niobium	[a].1	-----	.5	.3	-----	-----
Hafnium	-----	-----	.4	.1	-----	-----
Zirconium	.08	-----	-----	-----	-----	-----
Rhenium	-----	-----	.3	.1	-----	-----
Iron	[a].35	-----	-----	----	-----	-----
Carbon	.1	.47	.13	.66	.10	.47
Boron	.015	-----	-----	-----	-----	-----
Silicon	[a].25	-----	-----	-----	-----	-----
Manganese	[a].2	-----	-----	-----	-----	-----

[a]Maximum value.

Table II. - Summary of Chemical Mechanism of Hot Corrosion

Reactions occurring during induction period

1. $Cr_2O_3 + 3/2\ O_2 + 2Na_2SO_4(\ell) \rightarrow 2Na_2CrO_4(\ell) + 2SO_3(g)$

2. $MoO_3(\ell) + Na_2SO_4(\ell) \rightarrow Na_2MoO_4(\ell) + SO_3(g)$

End of induction period

3. $Ni + SO_4^{=} \rightarrow NiS(\ell) + 3/2\ O_2 + O^{=}$

4. $2Al + 3SO_4^{=} \rightarrow Al_2O_3 + 3SO_2(g) + 3O^{=}$

5. $2Cr + 3SO_4^{=} \rightarrow Cr_2O_3 + 3SO_2(g) + 3O^{=}$

Region of parabolic rate: Basic fluxing of protective Al_2O_3

6. $Al_2O_3 + O^{=} \rightarrow 2AlO_2^{-}$

Intermediate region

7. $MoO_3(\ell) + O^{=} \rightarrow MoO_4^{=}$

8. $MoO_3(\ell) + 2NaAlO_2 \rightarrow Al_2O_3 + Na_2MoO_4(\ell)$

9. $2MoO_3(\ell) + 2Na_2CrO_4 \rightarrow Cr_2O_3 + 2Na_2MoO_4(\ell) + 3/2\ O_2$

Region of linear rate: Acidic fluxing of protective Al_2O_3

10. $Al_2O_3 + 3MoO_3(\ell) \rightarrow 2Al^{+3} + 3MoO_4^{=}$

11. $NiS(\ell) + 3/2\ O_2 \rightarrow NiO + SO_2(g)$

Inhibiting effect of tantalum: During induction period

12. $Ta_2O_5 + Na_2SO_4(\ell) \rightarrow 2NaTaO_3 + SO_3(g)$

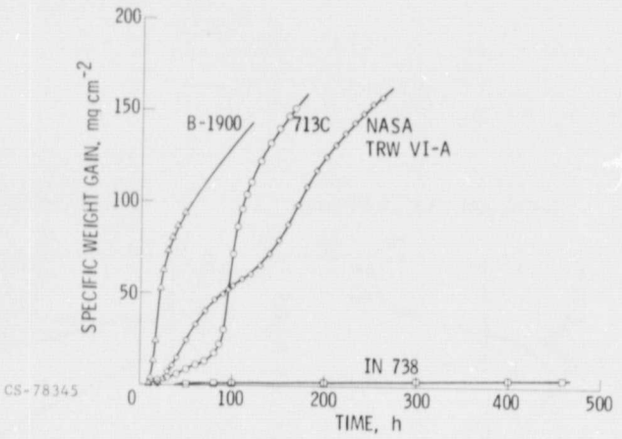

Figure 1. - Comparison of sodium sulfate-induced hot corrosion behavior of four nickel-base superalloys tested at 900° C. All specimens were preoxidized at 900° C for 100 hours in flowing oxygen and coated with 3 mg cm^{-2} Na_2SO_4 (Ref. 4) prior to hot corrosion test.

ΔW/A: 0.15 mg cm^{-2}
TIME: 4 h

3 mg cm^{-2}
7 h

CS-79-4274

Figure 2. - Preoxidized B-1900 with 3 mg cm^{-2} Na_2SO_4 tested at 900° C showing appearance of surface at different times of testing.

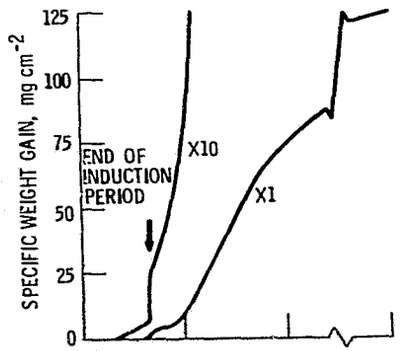

(a) TYPICAL WEIGHT CHANGE CURVE SHOWN AT TWO SENSITIVITIES.

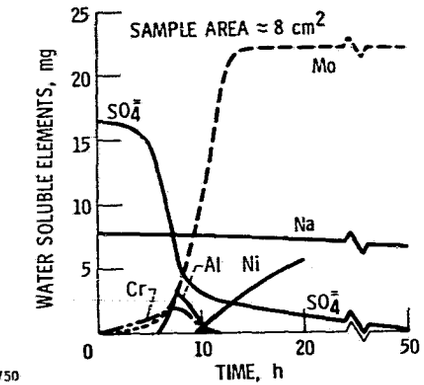

CS-79-3750

(b) AMOUNT OF WATER SOLUBLE ELEMENTS FOUND AFTER VARIOUS TIMES OF HOT CORROSION TESTING.

Figure 3. - Preoxidized B-1900 with 3 mg cm^{-2} Na_2SO_4, tested at 900° C.

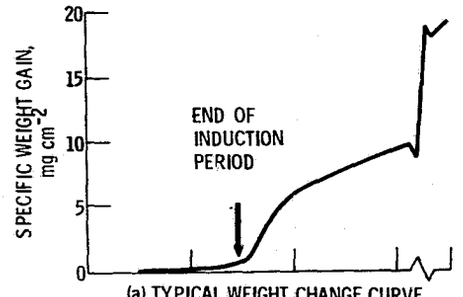

(a) TYPICAL WEIGHT CHANGE CURVE.

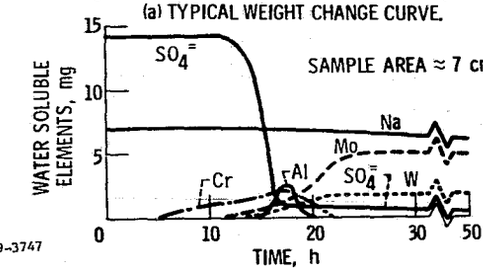

CS-79-3747

(b) AMOUNT OF WATER SOLUBLE ELEMENTS FOUND AFTER VARIOUS TIMES OF HOT CORROSION TESTING.

Figure 4. - Preoxidized NASA-TRW VIA with 3 mg cm^{-2} Na_2SO_4, tested at 900° C.

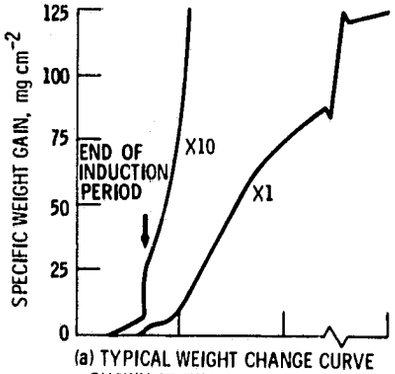

(a) TYPICAL WEIGHT CHANGE CURVE SHOWN AT TWO SENSITIVITIES.

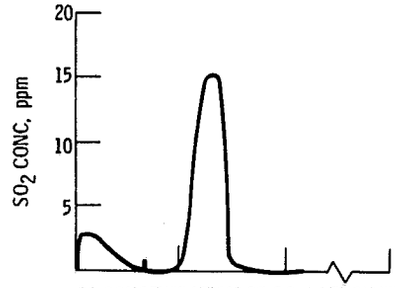

(b) CONCENTRATION OF SO_2(g) EVOLVED AS A FUNCTION OF TIME OF HOT CORROSION TESTING WITH AN OXYGEN FLOW RATE OF 620 cc min^{-1}.

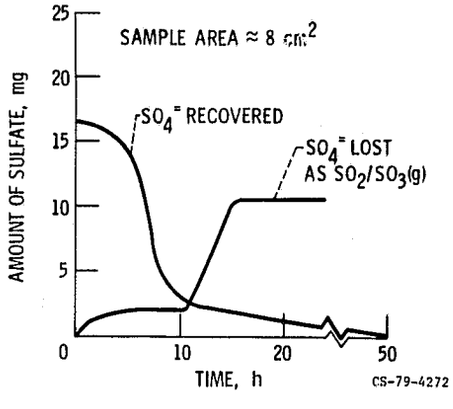

(c) COMPARISON OF THE AMOUNT OF WATER SOLUBLE $SO_4^=$ RECOVERED WITH EQUIVALENT $SO_4^=$ FROM SO_2/SO(g) EVOLVED.

Figure 5. - Preoxidized B-1900 with 3 mg cm^{-2} Na_2SO_4, tested at 900° C.

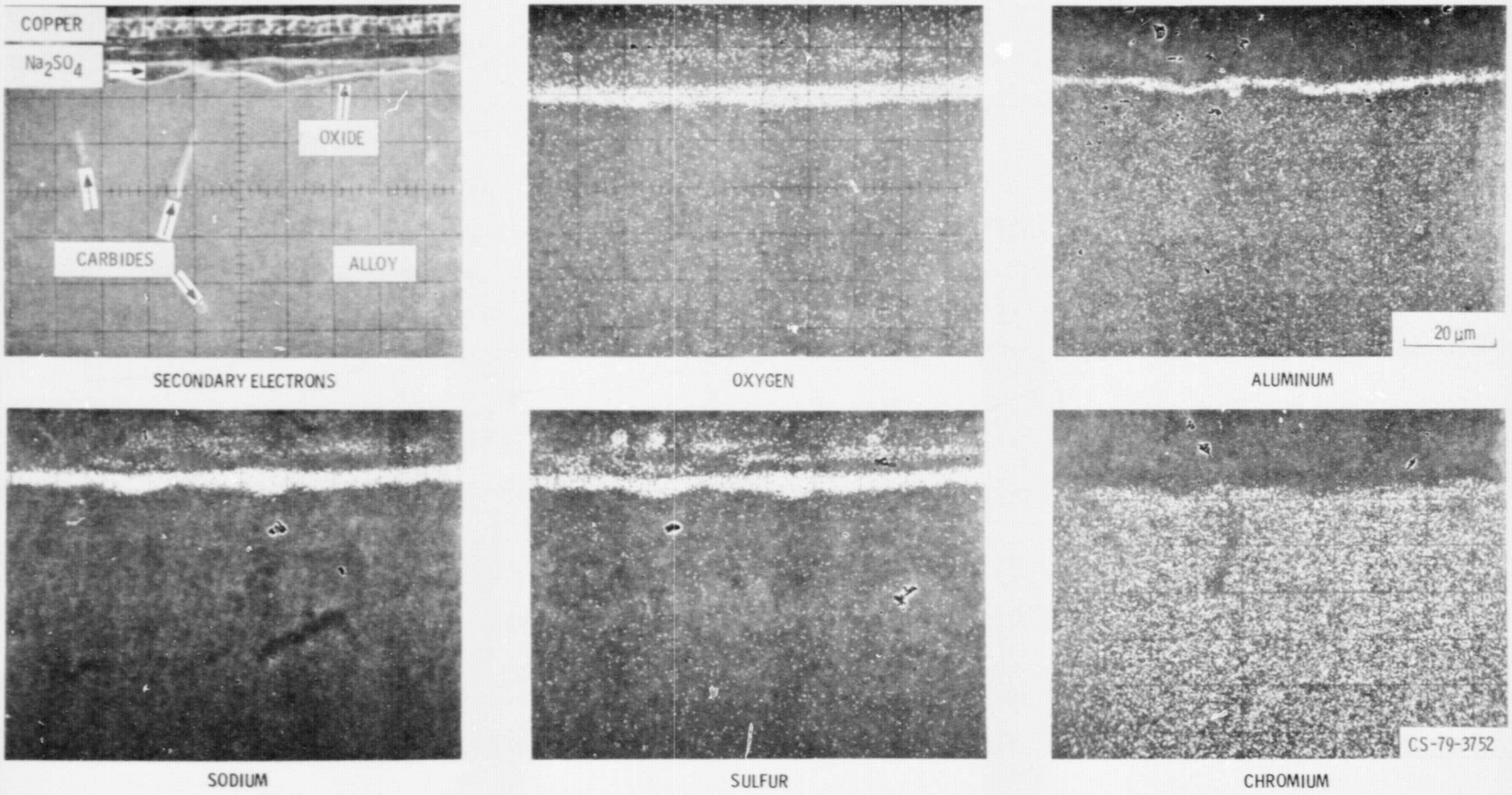

Figure 6. - Secondary electron micrograph and X-ray micrographs of preoxidized B-1900 sample corroded at 900° C with 3 mg cm^{-2} Na_2SO_4 for 15 minutes.

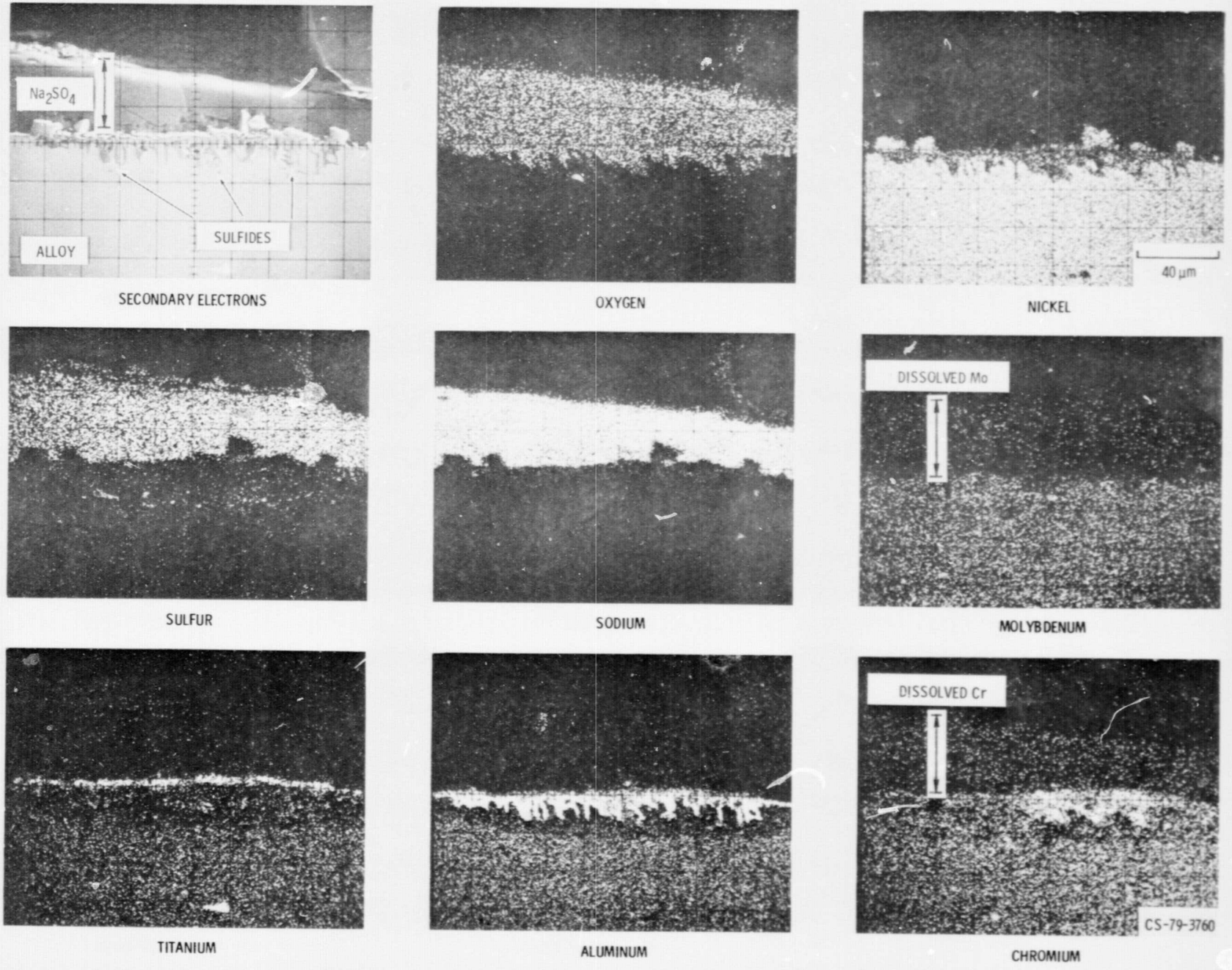

Figure 7. - Secondary electron micrograph and X-ray micrographs of preoxidized B-1900 sample corroded at 900^0 C with 3 mg cm^{-2} Na_2SO_4 for 3 hours.

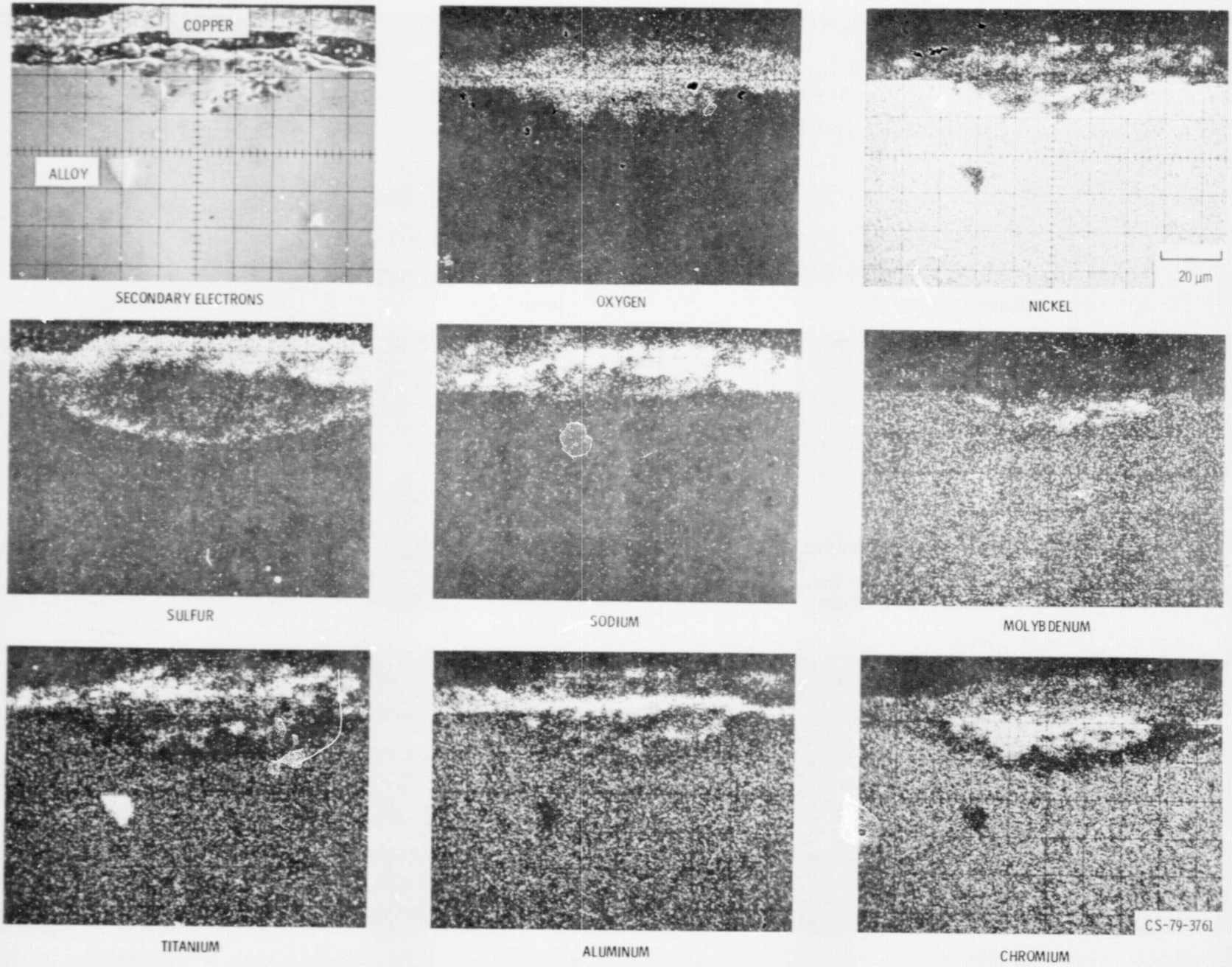

Figure 8. - Secondary electron micrograph and X-ray micrographs of preoxidized B-1900 sample corroded at 900^0 C with 3 mg cm^{-2} Na_2SO_4 for 4 hours.

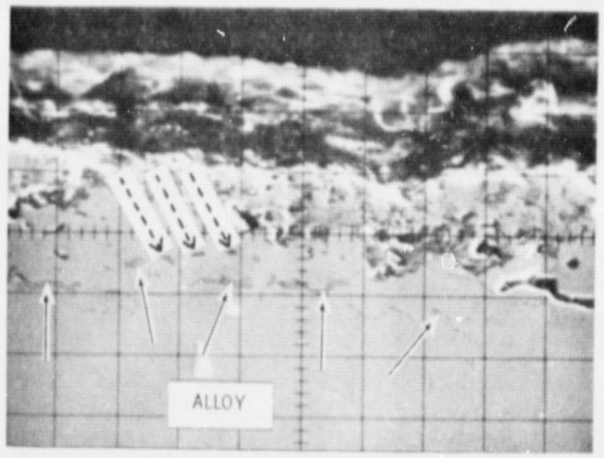

SECONDARY ELECTRONS

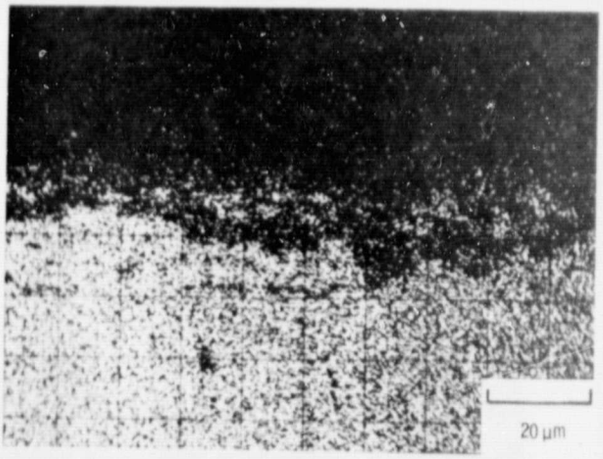

NICKEL

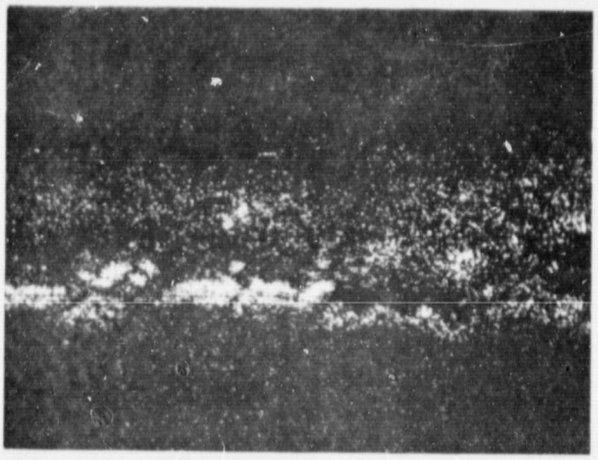

SULFUR

SODIUM

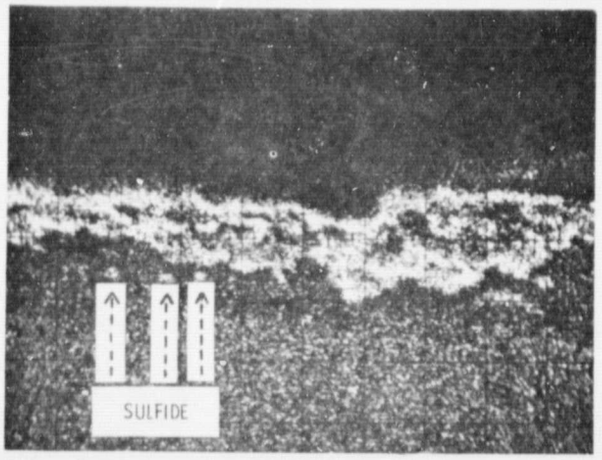

ALUMINUM

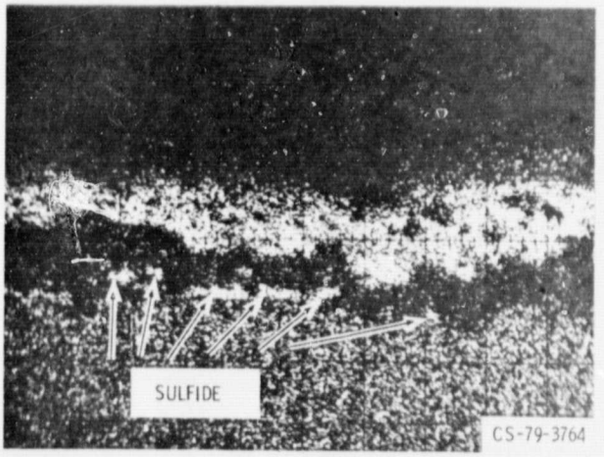

CHROMIUM

Figure 9. - Secondary electron micrograph and X-ray micrographs of preoxidized B-1900 sample corroded at 900° C with 3 mg cm^{-2} Na_2SO_4 for 5 hours. Arrows point out internal sulfides.

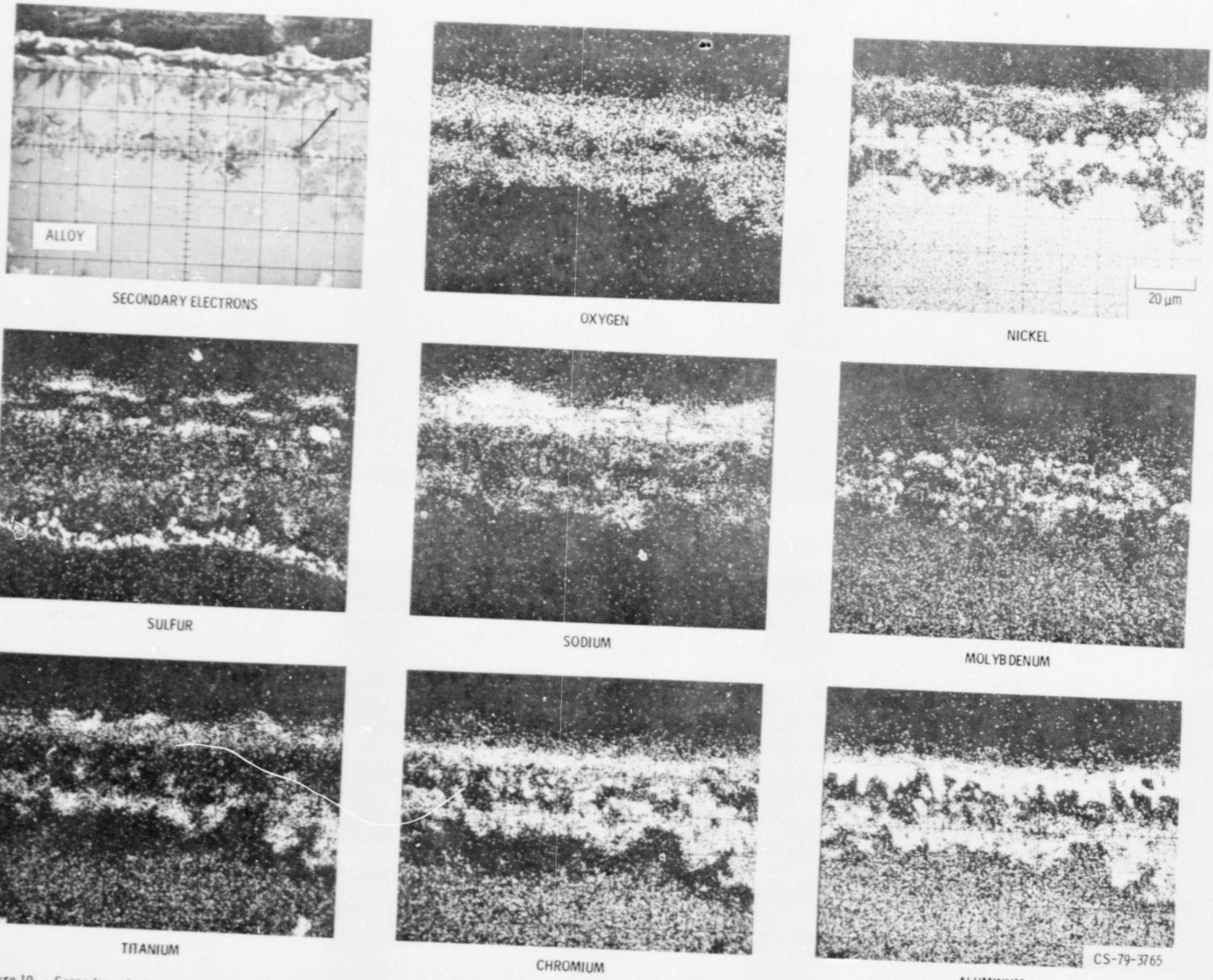

Figure 10. - Secondary electron micrograph and X-ray micrographs of preoxidized B-1900 sample corroded at 900° C with 3 mg cm^{-2} Na_2SO_4 for 6.25 hours. Arrow points out nickel sulfide particle in oxide scale.

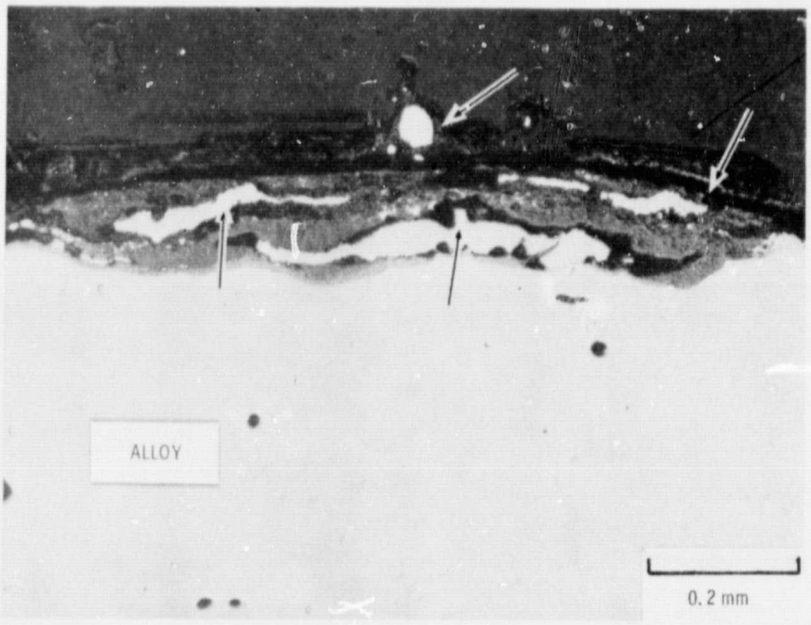

Figure 11. - Light micrograph of hot corrosion front on preoxidized B-1900 sample corroded at 900^0 C with 3 mg cm^{-2} Na_2SO_4 for 6.25 hours. Arrows point out nickel sulfide in oxide scale.

CS-79-3758

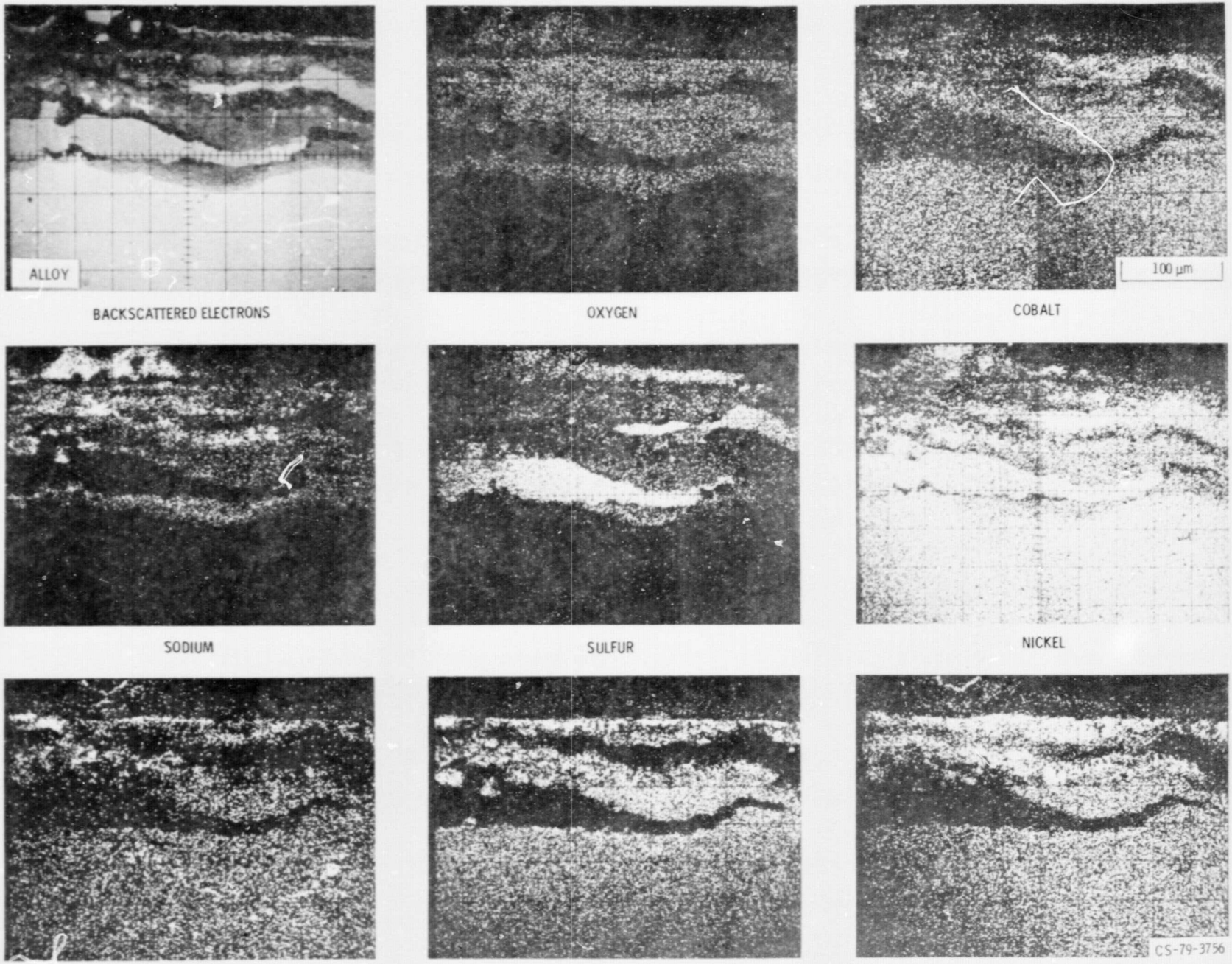

Figure 12. - Backscattered electron micrograph and X-ray micrographs of preoxidized B-1900 sample corroded at 900^0 C with 3 mg cm^{-2} Na_2SO_4 for 6.25 hours.

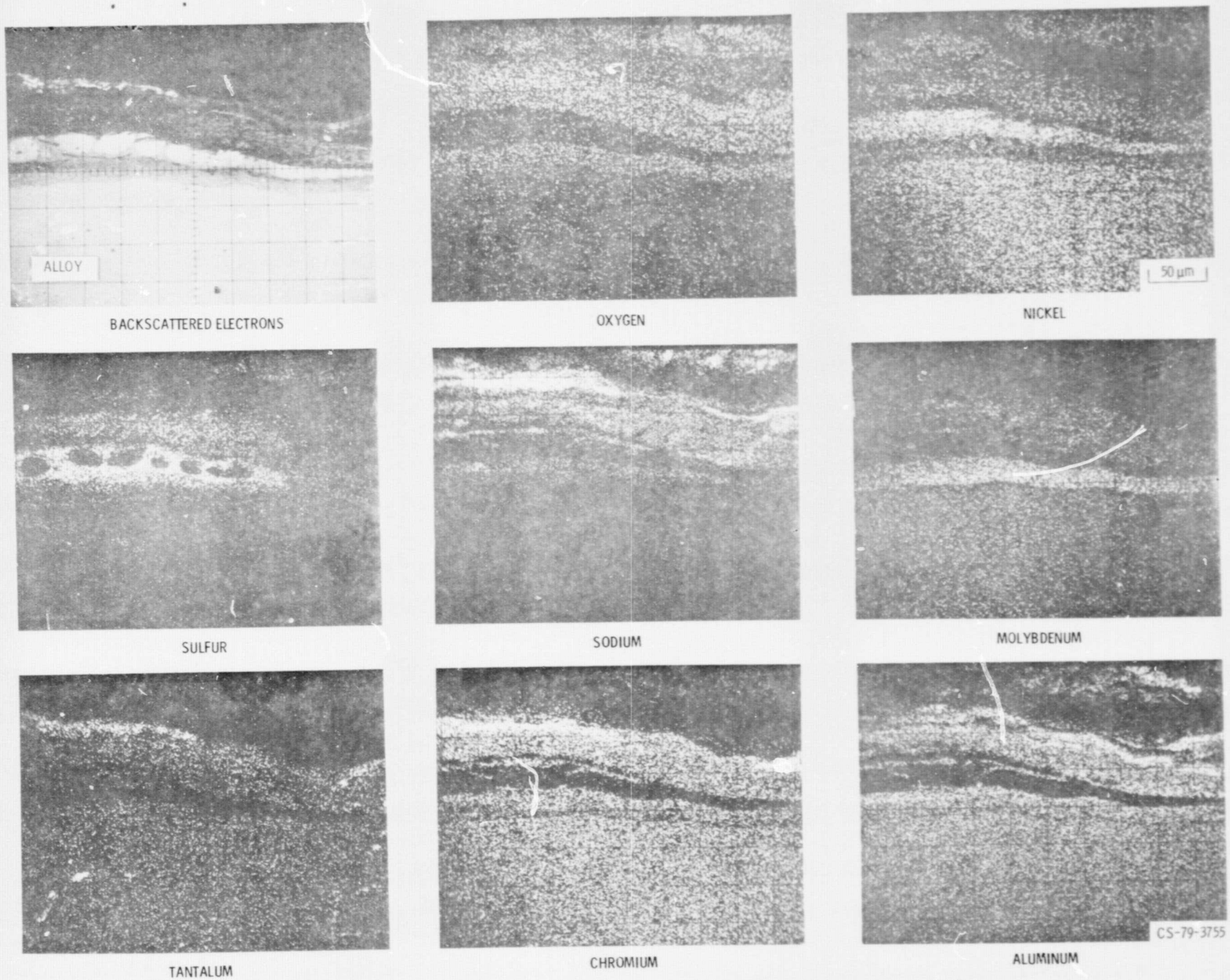

Figure 13. - Backscattered electron micrograph and X-ray micrographs of preoxidized B-1900 sample corroded at 900^0 C with 3 mg cm^{-2} Na_2SO_4 for 7 hours.

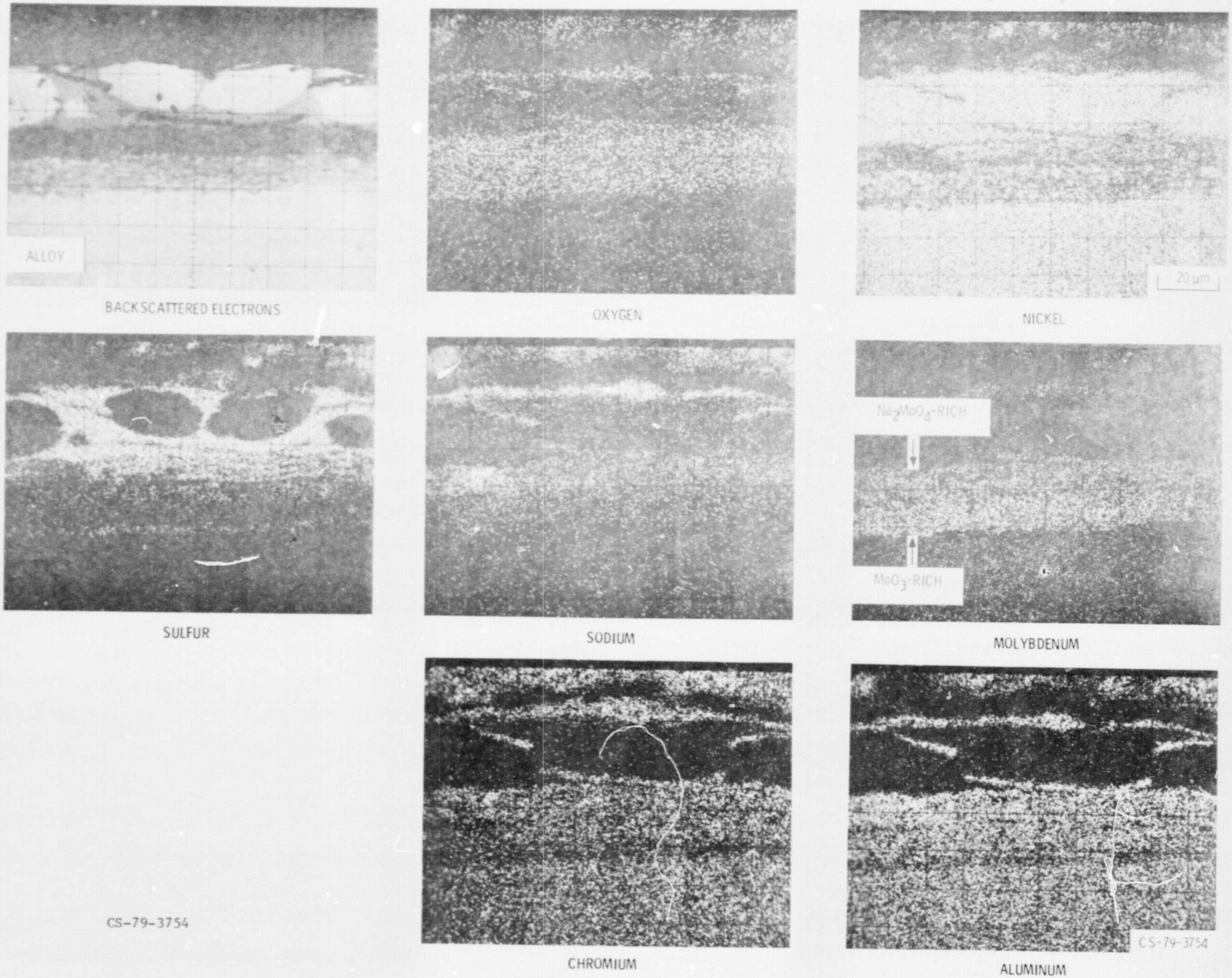

Figure 14. - Backscattered electron micrograph and X-ray micrographs of preoxidized B-1900 sample corroded at 900° C with 3 mg cm^{-2} Na_2SO_4 for 7 hours. Higher magnification of a portion of Figure 13.

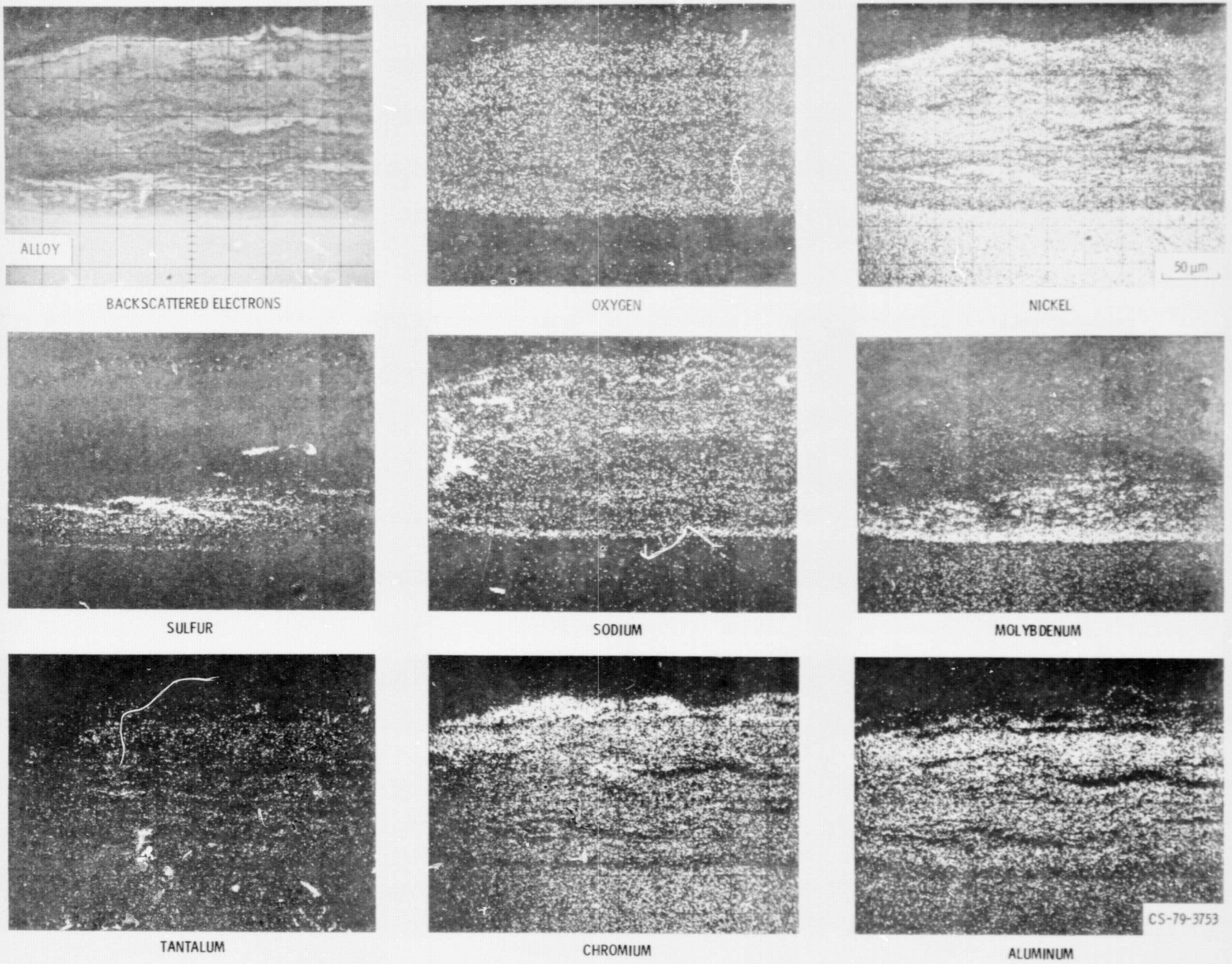

Figure 15. - Backscattered electron micrograph and X-ray micrographs of preoxidized B-1900 sample corroded at 900° C with 3 mg cm^{-2} Na_2SO_4 for 10 hours.

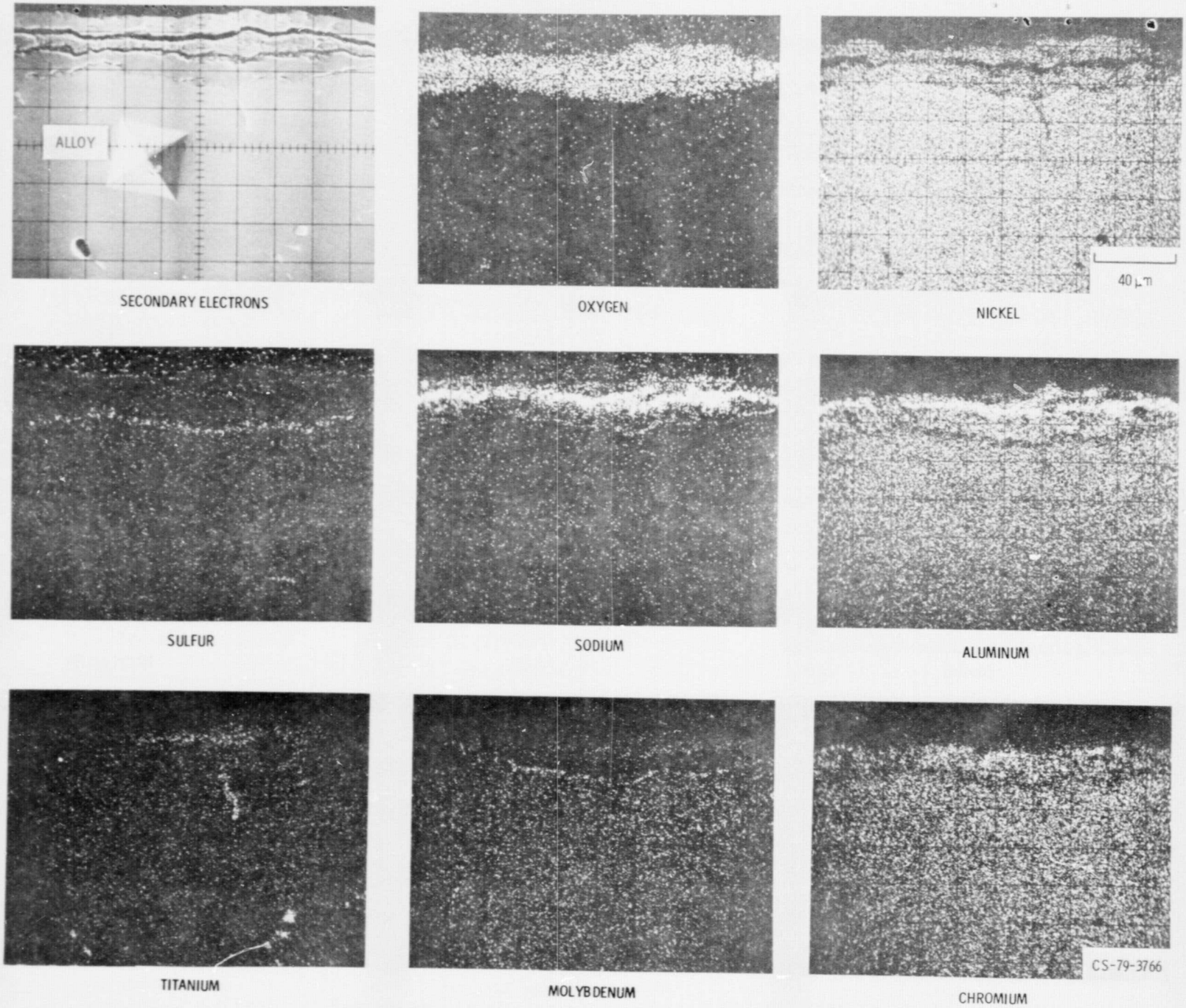

Figure 16. - Secondary electron micrograph and X-ray micrographs of preoxidized B-1900 sample corroded at 900^{0} C with 3 mg cm^{-2} Na_2SO_4 for 10 hours.

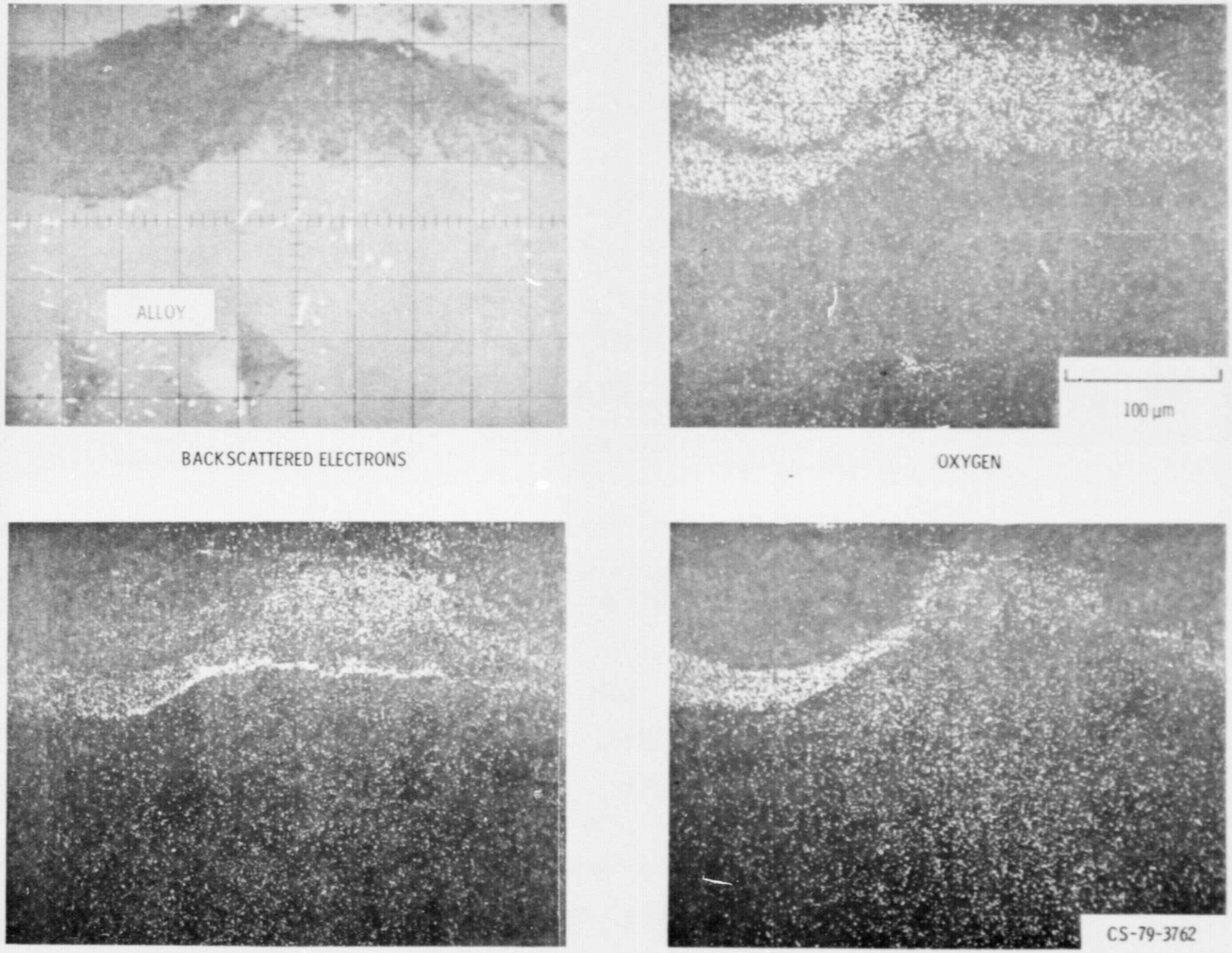

Figure 17. - Backscattered electron micrograph and X-ray micrographs of preoxidized B-1900 sample corroded at 900° C with 3 mg cm^{-2} Na_2SO_4 for 20 hours.

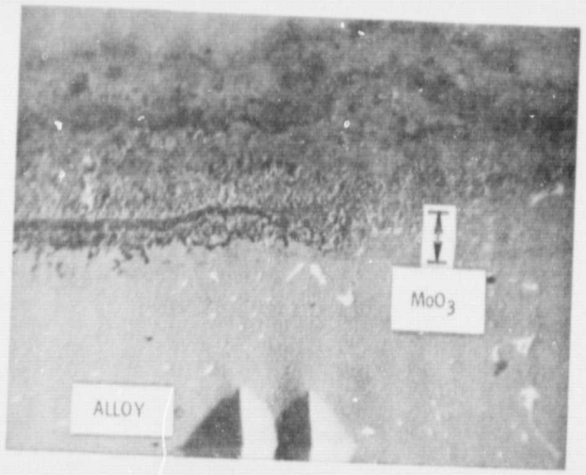

BACKSCATTERED ELECTRONS

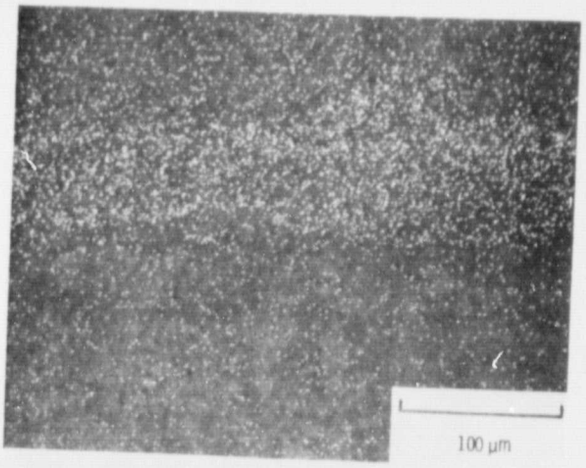

OXYGEN

SULFUR

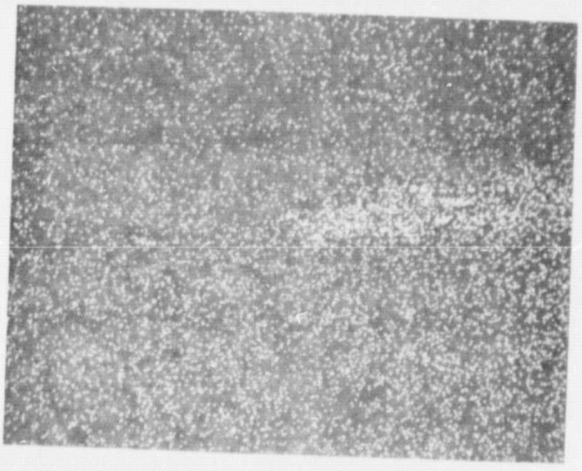

MOLYBDENUM

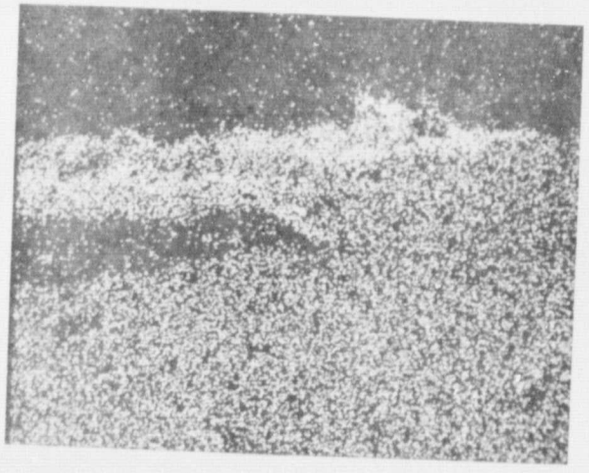

CHROMIUM

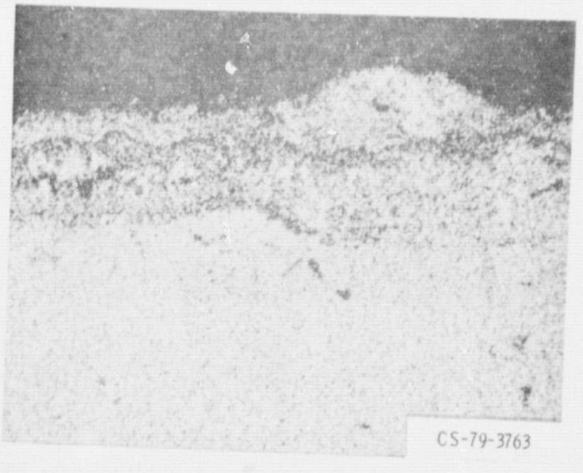

NICKEL

Figure 18. - Backscattered electron micrograph and X-ray micrographs of preoxidized NASA-TRW VIA sample corroded at 900° C with 3 mg cm^{-2} Na_2SO_4 for 17.5 hours.

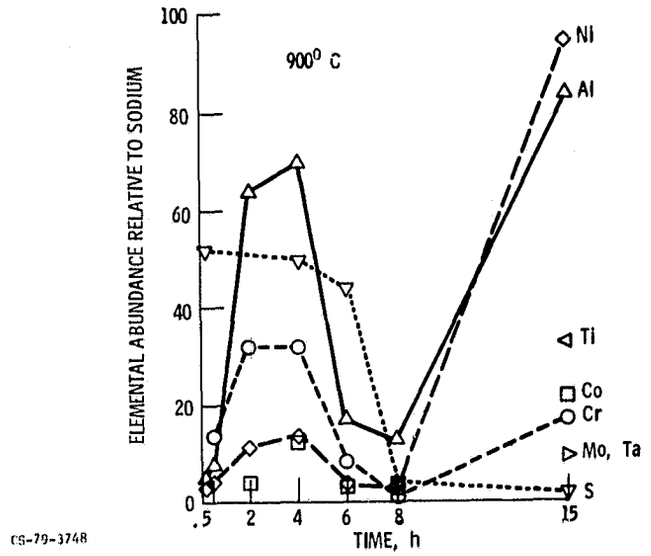

Figure 19. - ESCA analysis of preoxidized B-1900 samples corroded for various periods at 900° C with 3 mg cm^{-2} Na_2SO_4.

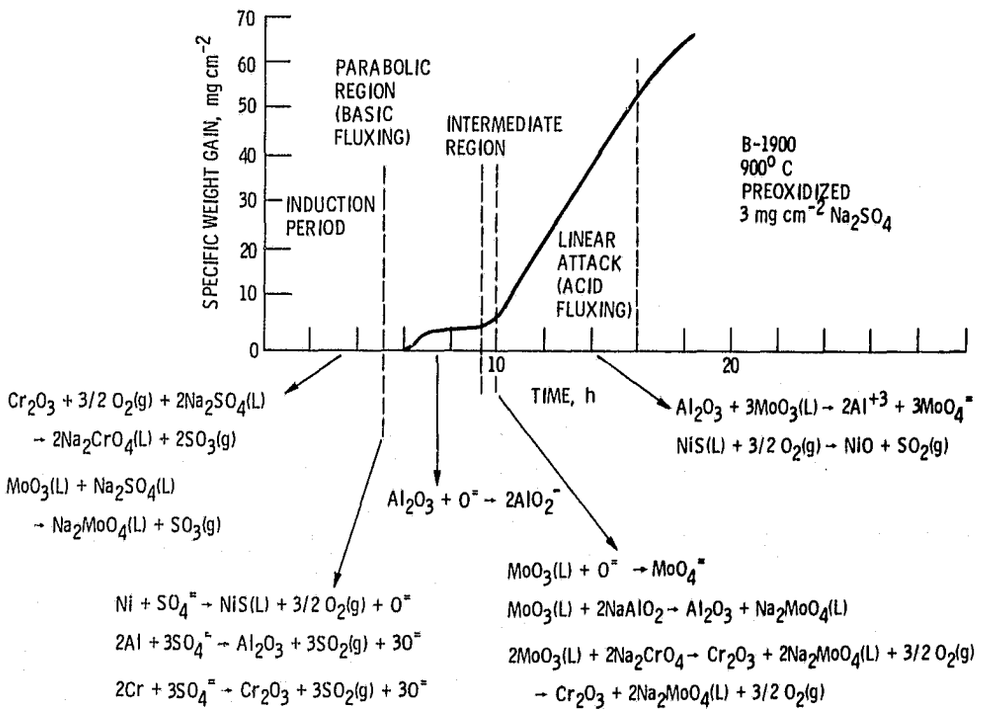

Figure 20. - Summary of chemical mechanism of hot corrosion.

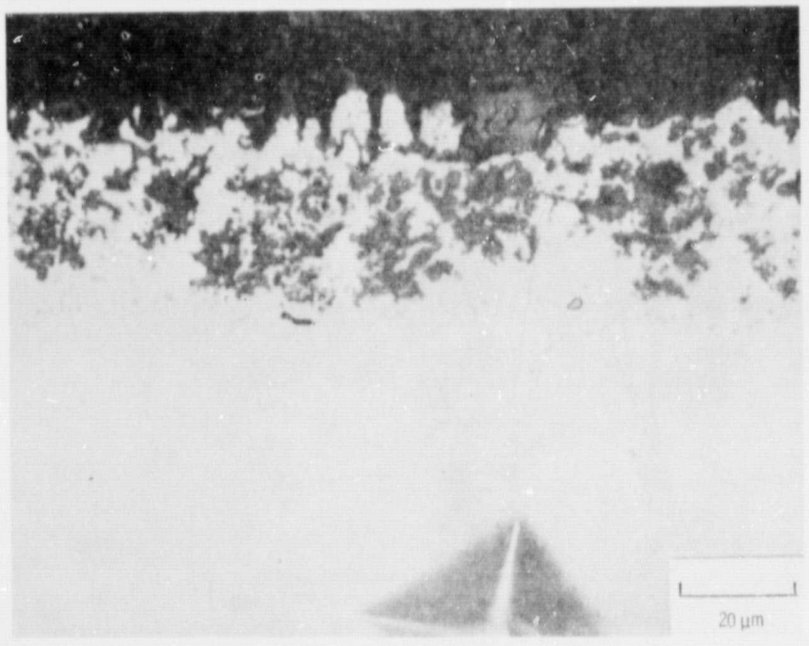

TIME: 6.25 h

(a) BASIC FLUXING.

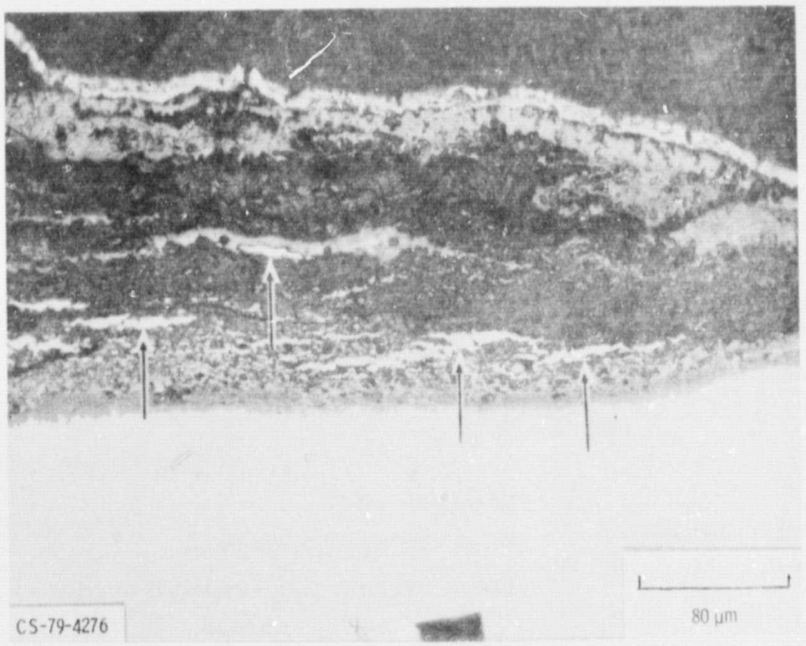

TIME: 10 h

(b) ACIDIC FLUXING.

Figure 21. - Light micrographs of scales formed on preoxidized B-1900 samples corroded for different times, illustrating examples of (a) basic fluxing and (b) acidic fluxing. Arrows point out nickel sulfide particles in the corrosion scale.

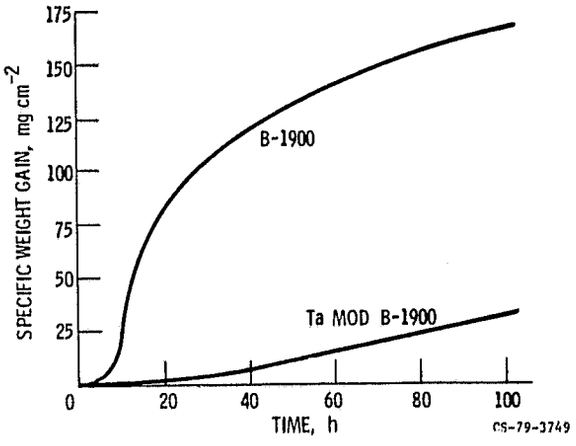

Figure 22. - Comparative hot corrosion behavior of B-1900 and Ta-modified B-1900 at 900^{0} C coated with 3 mg cm^{-2} Na_2SO_4. Samples were preoxidized at 900^{0} C in oxygen for 100 hours prior to hot corrosion test.

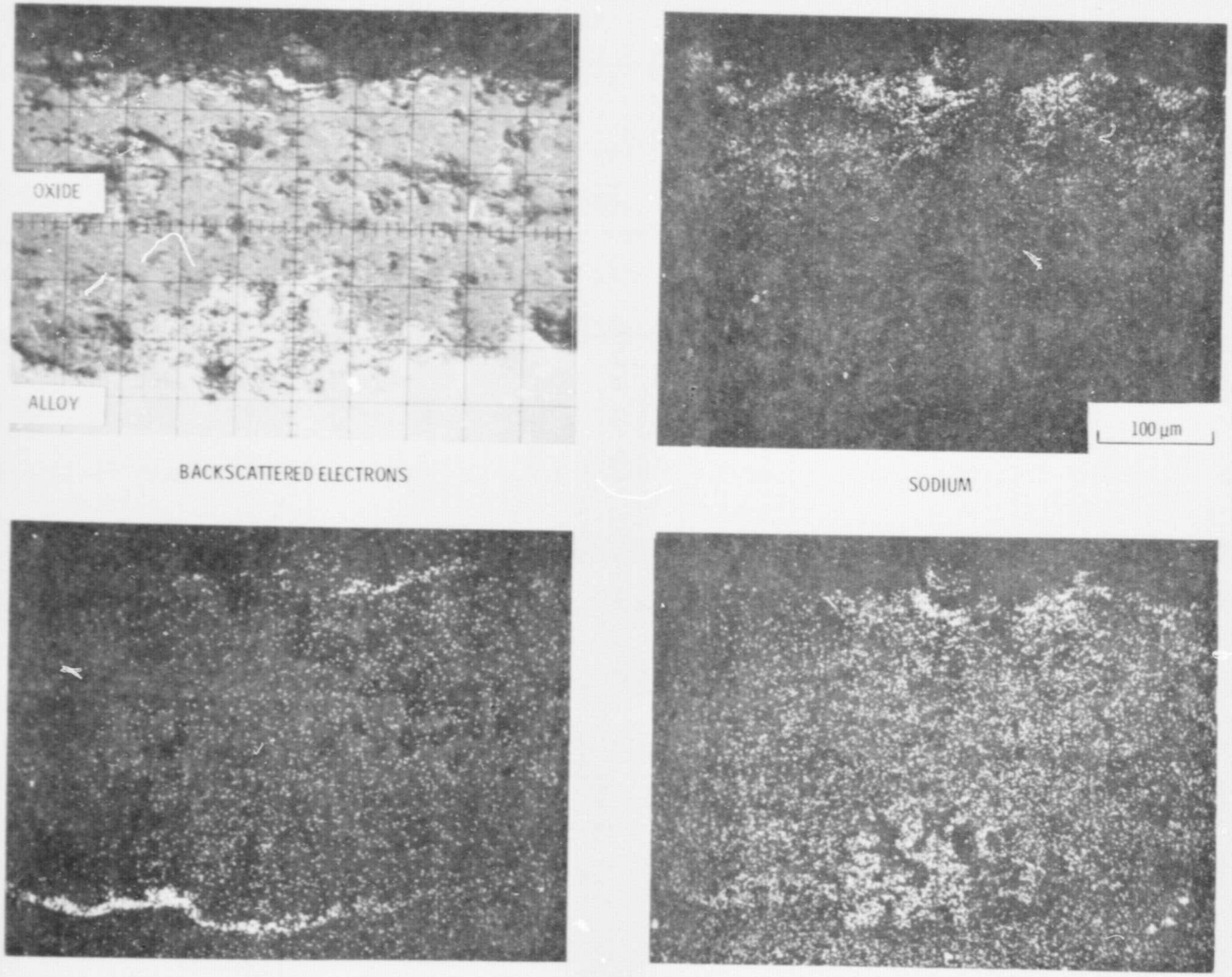

Figure 23. - Backscattered electron micrograph and X-ray micrographs of preoxidized Ta-modified B-1900 sample corroded at 900° C with 3 mg cm^{-2} Na_2SO_4 for 100 hours.

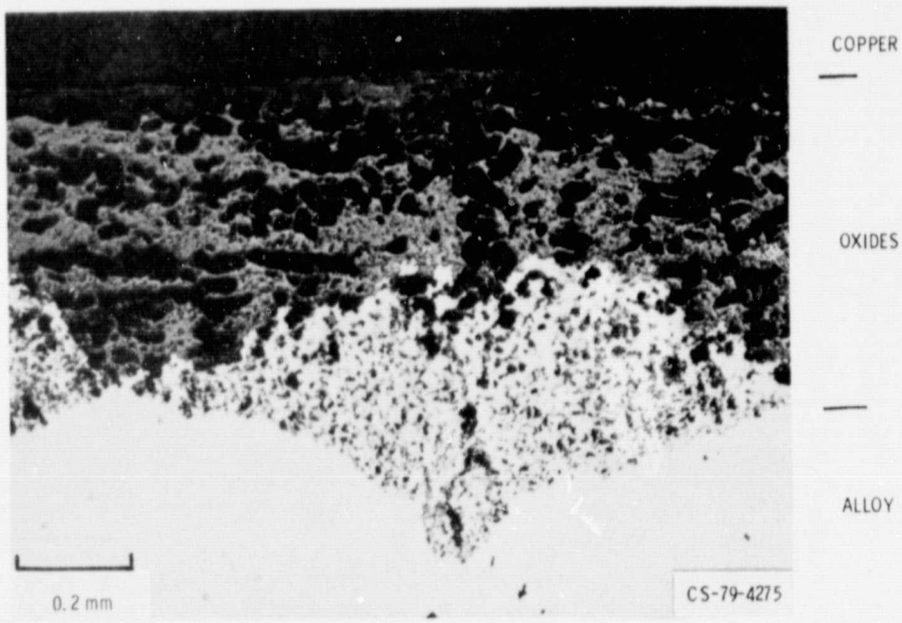

Figure 24. - Light micrograph of preoxidized Ta-modified B-1900 sample corroded at 900° C with 3 mg cm^{-2} Na_2SO_4 for 120 hours.

1. Report No. NASA TM-81399	2. Government Accession No.	3. Recipient's Catalog No.
4. Title and Subtitle **CHEMICAL PROCESSES INVOLVED IN THE INITIATION OF HOT CORROSION OF B-1900 AND NASA-TRW VIA**		5. Report Date 6. Performing Organization Code
7. Author(s) George C. Fryburg, Fred J. Kohl, and Carl A. Stearns		8. Performing Organization Report No. E-308 10. Work Unit No.
9. Performing Organization Name and Address National Aeronautics and Space Administration Lewis Research Center Cleveland, Ohio 44135		11. Contract or Grant No. 13. Type of Report and Period Covered Technical Memorandum
12. Sponsoring Agency Name and Address National Aeronautics and Space Administration Washington, D.C. 20546		14. Sponsoring Agency Code

15. Supplementary Notes

16. Abstract

Sodium sulfate-induced hot corrosion of B-1900 and NASA-TRW VIA at 900° C has been studied with special emphasis on the chemical reactions occurring during and immediately after the induction period. Thermogravimetric tests were run for set periods of time after which the samples were washed with water. Information was obtained by chemical analysis of water soluble metal salts and or residual sulfate. Companion samples were run, cross-sectioned dry, and polished in Varsol. Element distributions within the oxide layer were obtained from electron microprobe X-ray micrographs. A third set of samples was subjected to surface analysis by ESCA. Evolution of $SO_2(g)$ was monitored throughout many of the hot corrosion tests. Results are interpreted in terms of acid-base fluxing mechanisms.

17. Key Words (Suggested by Author(s))
Hot corrosion; Sodium sulfate; Nickel-base superalloys; Oxidation; Sulfides

18. Distribution Statement
Unclassified - unlimited
STAR Category 26

19. Security Classif. (of this report)	20. Security Classif. (of this page)	21. No. of Pages	22. Price*
Unclassified	Unclassified		

* For sale by the National Technical Information Service, Springfield, Virginia 22161